Methods for resolving the origin of large igneous provinces from crustal seismology

Jun Korenaga[1]

Department of Earth, Atmospheric, and Planetary Sciences, Massachusetts Institute of Technology, Cambridge, Massachusetts, USA

Peter B. Kelemen

Department of Geology and Geophysics, Woods Hole Oceanographic Institution, Woods Hole, Massachusetts, USA

W. Steven Holbrook

Department of Geology and Geophysics, University of Wyoming, Laramie, Wyoming, USA

[1]   We present a new quantitative framework to understand the process of mantle melting based on the velocity structure of igneous crust. Our approach focuses on the lower crustal section, which is expected to be least affected by porosity and seawater alteration, especially for thick igneous crust. Our methodology is thus best for constraining the origin of large igneous provinces. First, a quantitative relation between bulk crustal velocity and mantle melting parameters is established on the basis of data from mantle melting experiments. Second, we show how lower crustal velocity can be used to place bounds on the expected range of bulk crustal velocity, despite ambiguity in crustal emplacement processes. By modeling fractional crystallization processes at a range of crustal pressures, these bounds are derived as a function of the proportion of lower versus upper crust. Finally, a simple mantle melting model is constructed to illustrate the effects of potential temperature, active upwelling, and a preexisting lithospheric lid on predicted crustal thickness and velocity. As an example, this new interpretation is applied to a seismic transect across the southeast Greenland margin to constrain mantle dynamics during the opening of the North Atlantic. Some complicating factors in seismological inference on mantle melting process, such as the possibilities of subcrustal igneous fractionation and mantle source heterogeneity, are also discussed with this example.   *INDEX TERMS:* 7220 Seismology: Oceanic crust; 3640 Mineralogy and Petrology: Igneous petrology; 3035 Marine Geology and Geophysics: Midocean ridge processes; 8121 Tectonophysics: Dynamics, convection currents and mantle plumes; *KEYWORDS:* lower crust, mantle melting, mantle plumes, igneous fractionation, mantle source heterogeneity, North Atlantic igneous province

1. Introduction

[2] Large igneous provinces (LIPs) are products of unusually extensive magmatism, with respect to the "normal" state of terrestrial magmatism such as is observed at the majority of mid-ocean ridges [e.g., *Coffin and Eldholm*, 1994]. Though LIPs are the largest expression of magmatism on this planet, their origins are still poorly understood. Plumes derived from the lower mantle have been the most commonly accepted explanation for focused supply of mantle-derived melt [e.g., *Richards et al.*, 1989; *White and McKenzie*, 1989; *Hill et al.*, 1992], whereas relatively shallow, small-scale convection as a result of surface tectonics has also been advocated as a possible explanation [e.g., *Mutter et al.*, 1988; *Anderson*, 1994; *Boutilier and Keen*, 1999]. Given our limited understanding of realistic mantle dynamics, especially when melting is involved [e.g., *Cordery and Phipps Morgan*, 1993; *Tackley and Stevenson*, 1993; *Spiegelman*, 1996; *Braun et al.*, 2000], it is difficult at present to distinguish different hypotheses solely by commonly employed arguments based on geological coincidence (e.g., plume head impacts for LIPs and plume tails for succeeding hot spot chains). Obtaining quantitative constraints on basic parameters, such as the potential temperature of mantle and its upwelling rate, is an essential step in investigating the formation of LIPs as well as improving our understanding of multiscale mantle dynamics.

---

[1]Now at Department of Earth and Planetary Science, University of California, Berkeley, California, USA.

[3] The temperature and upwelling rate of the mantle are reflected in the composition and volume of melt generated by adiabatic decompression. Since seismic velocity is sensitive to rock composition, the velocity structure of resultant igneous crust can, in principle, provide robust constraints on the composition of mantle-derived melt, from which we can estimate past mantle dynamics. In particular, for LIPs formed near divergent plate boundaries where lithospheric controls on melt migration may be minimal, the whole crustal velocity structure is a promising proxy for parental melt composition [*Kelemen and Holbrook*, 1995]. There have been, however, two critical difficulties with this inference. The first difficulty is with the reliability of crustal velocity models. Because basaltic upper crust is usually highly porous and seismic velocity is more sensitive to porosity structure than to composition, only the lower crust remains useful for petrological interpretation. The seismic structure of the lower crust is, however, more difficult to confidently determine; Moho reflection travel times are often the sole seismic constraint when crust is thick, so accurate determination of lower crustal velocity tends to be hindered by uncertainties in Moho depth. In addition, because uncertainty analysis for velocity models has often been incomplete, owing to the nonlinear nature of tomographic inversions, it is hard to assess the accuracy of resulting petrological interpretations. A means of resolving the difficulties in estimating lower crustal velocity and its uncertainty is to use joint refraction and reflection tomography with a comprehensive uncertainty analysis such as that formulated by *Korenaga et al.* [2000].

[4] The second difficulty lies in the estimation of parental mantle melt from crustal seismic velocity. *Kelemen and Holbrook* [1995] conducted an early, quantitative attempt to estimate the volume and composition of mantle melt from crustal velocity structure. They replaced upper crustal velocity uniformly with 6.8 km s^{-1} to minimize the effects of porosity and alteration, and calculated the whole crustal average velocity to estimate bulk crustal composition. It is difficult, however, to test the assumption of uniform upper crustal velocity (and composition), so errors in the averaged velocity introduced by this assumption are uncertain. It is also assumed that material with velocities above 6.8 km s^{-1} is unaltered.

[5] The purpose of this paper is to construct a more robust framework for interpreting the seismic structure of igneous crust. We decided upon a different approach, using only lower crustal velocity to estimate parental magma composition. However, the relationship between upper and lower crustal compositions and parental melt composition can be complicated because of possible fractionation and assimilation processes during crustal accretion. Figure 1 shows some proposed crustal accretion models for normal oceanic crust. Modification of mantle-derived melt ascending through a crustal section is controlled by the thermal structure of crust, which depends on the balance of heating by magma injection and cooling by hydrothermal circulation and conductive heat loss [e.g., *Sleep*, 1991; *Phipps Morgan and Chen*, 1993]. Whereas slow spreading ridges have low-temperature axial crust, which may often lead to in situ crystallization of incoming batches of melt (Figure 1c), fast spreading ridges tend to have steady state axial magma chambers, in which crystal

fractionation can take place (Figures 1a and 1b). Although the importance of crustal thermal structure in modifying melt composition is generally accepted [e.g., *Sinton and Detrick*, 1992], how oceanic crust is actually constructed is controversial [*Boudier et al.*, 1996; *Kelemen et al.*, 1997b; *Chen*, 1998; *Kelemen and Aharonov*, 1998; *Korenaga and Kelemen*, 1998]. Our understanding of crustal and mantle thermal structure is even more limited during transient events such as continental breakup. Because of this uncertainty in the degree of lower crustal crystal fractionation, it is impossible to uniquely determine bulk composition from lower crustal velocity structure alone. Instead, we must seek to place reasonable bounds on the bulk composition.

[6] Fractionation processes depend mostly on melt composition, crystallization pressure, and the mode of fractionation (fractional and equilibrium crystallization). Any specific assumption regarding these factors must be avoided. Our approach is based on crystallization modeling at a range of crustal pressures using extensive experimental data sets on mantle melt composition at various temperatures and pressures. After establishing velocity-composition systematics, we then consider a mantle melting process incorporating the effects of active mantle upwelling and preexisting lithospheric lid, to explore possible variations in predicted crustal thickness and velocity. The potential significance of residual cracks in the seismic structure of normal oceanic crust is also discussed. Finally, we apply this new interpretation framework to the crustal velocity model of *Korenaga et al.* [2000] for the southeast Greenland margin, in terms of mantle melting and crustal accretion processes associated with the opening of the North Atlantic.

2. Mineralogies, Seismic Velocities, and Densities of Igneous Lower Crust

[7] The seismic structure of igneous crust usually has two distinct components: (1) the upper crustal section with a large velocity gradient, and (2) the lower crustal section with little or no velocity gradient. In this paper, we use these definitions. Though the petrological interpretation of this seismic layering is questionable owing to the uncertainties in crustal accretion processes (e.g., Figure 1), it is now generally believed that the large velocity variation in upper crust is caused by porosity and alteration [e.g., *Detrick et al.*, 1994], which do not strongly affect the lower crust.

[8] In this section, we develop relationships among lower crustal seismic velocity, the composition of primary mantle melts, and mantle melting processes. We introduce the terms bulk crustal velocity and norm-based velocity, both of which are somewhat hypothetical in a sense that they cannot be observed in actual seismic velocity models. As we will show, however, these notions are very useful in connecting observable lower crustal velocity to the composition of primary mantle melts.

2.1. Fractional Crystallization Processes and Bulk Crustal Velocity

[9] Igneous accretion processes in the lower crust may range from in situ crystallization of parental melt to cumulate formation by fractional crystallization. In this context, we define a "cumulate" as a rock that forms via partial
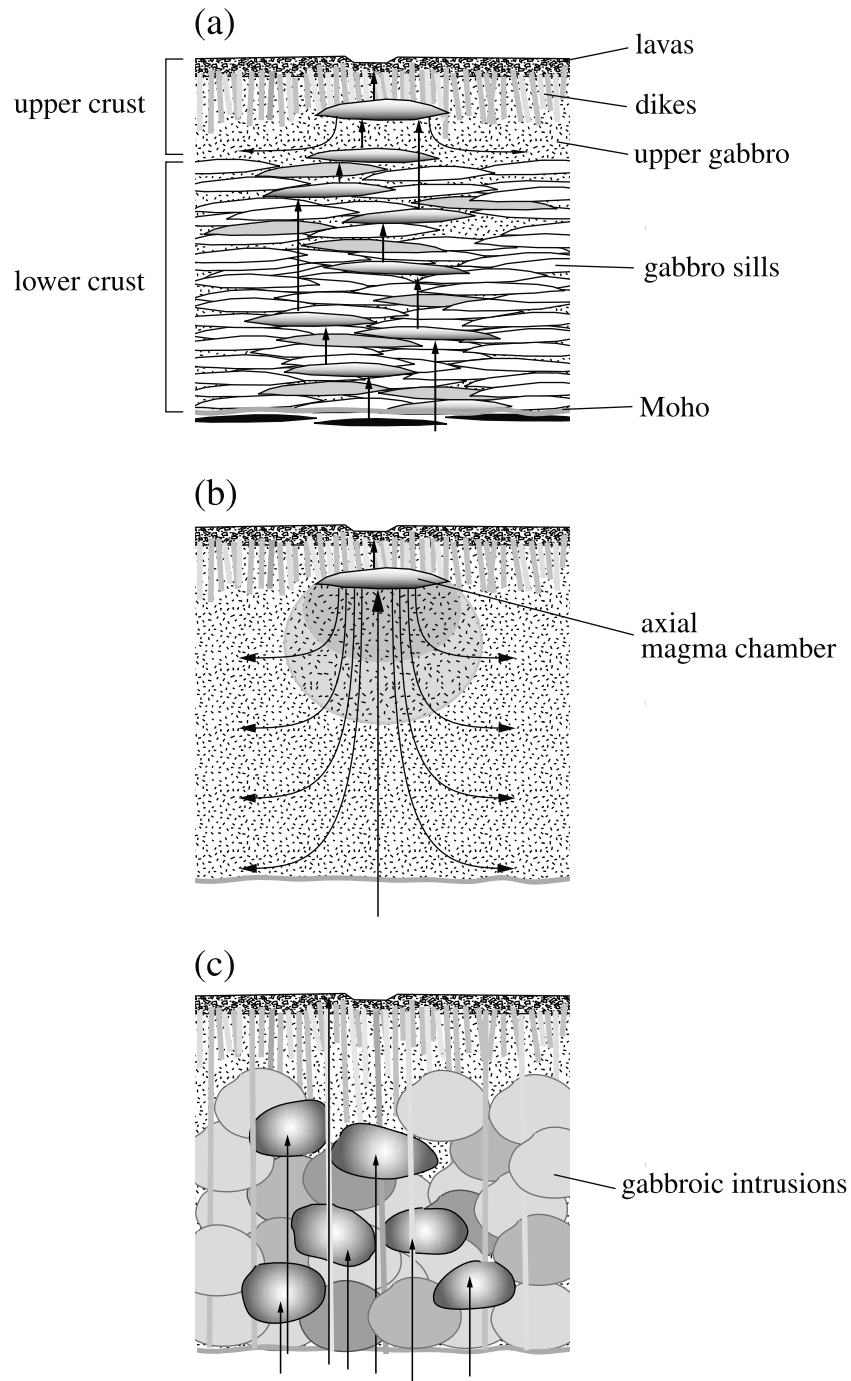
Figure 1. Schematic drawings for recently proposed accretion models for igneous crust. (a) Sheeted sill model [*Kelemen et al.*, 1997b; *Kelemen and Aharonov*, 1998], (b) gabbro glacier model [*Nicolas et al.*, 1988; *Henstock et al.*, 1993; *Phipps Morgan and Chen*, 1993; *Quick and Denlinger*, 1993; *Menke and Sparks*, 1995], and (c) intrusion model [*Dick et al.*, 1992; *Cannat*, 1996]. Models in Figures 1a and 1b are for fast spreading ridges while the model in Figure 1c is for slow spreading ridges.

crystallization of a melt, after which the remaining melt is removed from the system of interest. Because igneous cumulates commonly have more MgO than their parental liquids, and because rocks with higher MgO have higher seismic velocity, cumulate lower crust formed by fractional crystallization should have the highest velocity of all possible crystallization products from a given parental melt composition, thus providing an upper limit on the deviation of lower crustal velocity from bulk crustal velocity. Throughout this paper, we use the term "bulk crustal velocity" to denote a hypothetical crustal velocity corresponding to the case of 100% equilibrium crystallization of a primary, mantle-derived melt.

[10] The uncertainty in the estimation of parental melt composition from lower crustal velocity thus depends on the magnitude of the difference between the velocity of possible

cumulates and the velocity of rocks produced by equilibrium crystallization of primary melts. We constrain this difference by modeling fractional crystallization processes. We use the method of *Weaver and Langmuir* [1990] as extended by *Langmuir et al.* [1992] for high-pressure crystallization. Though actual crustal fractionation processes are probably more complex, including periodically replenished magma chambers [*O'Hara*, 1977], combined wall-rock assimilation and fractional crystallization [*DePaolo*, 1981], and in situ fractionation [*Langmuir*, 1989], the case of pure fractional crystallization provides an upper limit on lower crustal seismic velocity.

[11] Major crystallizing minerals from low-H_2O, primitive basaltic liquids at ≤ 1 GPa are olivine, plagioclase, and clinopyroxene, and the predicted crystallizing assemblages range from dunite to gabbro. The elastic properties of minerals depend on temperature, pressure, and composition. We use the compilation of *Sobolev and Babeyko* [1994] to calculate effective isotropic moduli and density at a given temperature and pressure for each mineral with a certain composition, and then calculate the Hashin-Shtrikman bounds [e.g., *Hashin and Shtrikman*, 1963; *Watt et al.*, 1976; *Berryman*, 1995] for the compressional wave velocity of a multi-phase solid assemblage. For mafic mineral assemblages, the bounds are typically tighter than 0.03 km s^{-1}, so that the average of the upper and lower bounds is sufficient for our purposes. We calculate hypothetical solid velocities for primary and residual liquids in a manner similar to that of *White and McKenzie* [1989]; the weight proportions of minerals and their compositions are calculated based on the CIPW norm [e.g., *Philpotts*, 1990, Chapter 6], the weight proportions are converted to the volume proportions using mineral densities, and effective compressional velocities of their assemblages are calculated in the same manner as for crystallizing assemblages. Hereafter we will refer to this velocity based on the CIPW norm as the "norm-based velocity". Although in principle the use of the CIPW norm may not be as accurate as thermodynamic calculations for estimating equilibrium mineral assemblages [e.g., *Sobolev and Babeyko*, 1994], norm-based velocity for bulk crustal composition can serve as a useful, easily reproduced reference to evaluate the influence of fractionation on lower crustal velocity.

[12] An example of crystallization modeling is shown in Figure 2. The starting liquid composition is an estimate of primary melt for normal mid-ocean ridges as calculated by *Kinzler* [1997] (polybaric near-fractional melt aggregated from a so-called "triangular shaped melting regime", with mean melt fraction of 9% and mean pressure of melting of 1.5 GPa). Three different crystallization paths are shown in this example: (1) fractional crystallization at 100 MPa, (2) polybaric fractional crystallization from 800 MPa to 100 MPa, and (3) equilibrium crystallization at 100 MPa. Compressional wave velocities of crystallizing phases as well as of residual phases are calculated as a function of the solid fraction (Figure 2a). The velocities are calculated at 100 MPa and 100°C, i.e., a typical midcrustal state of normal oceanic crust. For fractionally crystallizing phases, velocities are shown for both incremental and cumulative assemblages, the latter being of primary interest because of its relevance to average lower crustal velocity. Corresponding densities are also shown in Figure 2b, with densities of residual liquid

calculated by the method of *Bottinga and Weill* [1970]. Though the residual liquids become progressively denser with crystal fractionation, they are always more buoyant than the solid phases, so that the lower crust does not act as a density filter [e.g., *Sparks et al.*, 1980; *Stolper and Walker*, 1980] in this example. Higher crystallization pressure increases the stability of clinopyroxene [e.g., *Bender et al.*, 1978; *Presnall et al.*, 1978; *Grove et al.*, 1992] (Figure 2d), leading to a slight reduction in the velocity of the resultant assemblage (Figure 2a). Olivine is the sole crystallizing phase at early fractionation stages (Figures 2c–2e), and mostly because of this, the deviation of the maximum lower crustal velocity from the bulk crustal velocity ($\sim$7.17 km s^{-1} in this case) is too large to be useful when lower crust comprises only a small fraction of the whole crust. The deviation sharply decreases, however, at $\sim$20% solidification. In fact, the fraction of the lower crust is usually greater than 50% in igneous crust [e.g., *Mutter and Mutter*, 1993].

2.2. Primary Mantle Melts and Melting Systematics

[13] To establish a general relation between the norm-based bulk crustal velocity and lower crustal velocity of igneous crust using the bounding approach outlined above, a reasonably wide range of mantle melt compositions needs to be considered. We therefore compiled recent, high-quality melting experiments of mantle peridotites [*Kinzler and Grove*, 1992; *Hirose and Kushiro*, 1993; *Kinzler and Grove*, 1993; *Baker and Stolper*, 1994; *Kinzler*, 1997; *Walter*, 1998]. A norm-based velocity is calculated for each melt composition. The norm-based velocities of the compiled melt compositions at a pressure of 600 MPa and a temperature of 400°C (we will refer to this as the reference state) vary from 6.8 km s^{-1} to 7.8 km s^{-1} (Figure 3). In addition to these published melt data, we also calculated the composition of isobaric batch melts of depleted pyrolite mantle for pressures of 1–3 GPa and melt fraction ranging from 0.02 to 0.2, using the method of *Kinzler* [1997], and used them to supplement composition-velocity systematics. Since we are interested in a connection between the process of mantle melting and resultant igneous crustal structure, following the approach of *Kelemen and Holbrook* [1995] (hereafter referred to as KH95), the compressional wave velocities for mantle melts are related to their pressures and degrees of melting using multiple linear regression as (Figure 3),

$$V_p = a_0 + W_L(P,F)(b_0 + b_1 P + b_2 F + b_3 P^2 + b_4 PF + b_5 F^2)$$
$$+ W_H(P,F)(c_0 + c_1 P + c_2 F + c_3 P^2 + c_4 PF + c_5 F^2) \quad (1)$$

where P is the pressure of melting in GPa, F is melt fraction, and $a_0 = 7.52$, $b_0 = -1.73$, $b_1 = 0.55$, $b_2 = 7.71$, $b_3 = -0.11$, $b_4 = 8.87$, $b_5 = -146.11$, $c_0 = -0.35$, $c_1 = 0.034$, $c_2 = 0.51$, $c_3 = 0.0016$, $c_4 = -0.040$, and $c_5 = 0.046$. $W_L(P, F)$ and $W_H(P, F)$ are hypertangent window functions defined as

$$W_L(P,F) = \frac{1}{4}\{1 - \tanh[\alpha(P - P_t)]\}\{1 - \tanh[\beta(F - F_t)]\}$$

$$W_H(P,F) = \frac{1}{4}\{1 + \tanh[\alpha(P - P_t)]\}\{1 + \tanh[\beta(F - F_t)]\}$$

where $\alpha = 0.6$, $\beta = 8.4$, $P_t = 1.0$, and $F_t = 0.05$. This form of equation may seem too complicated, but it is needed to
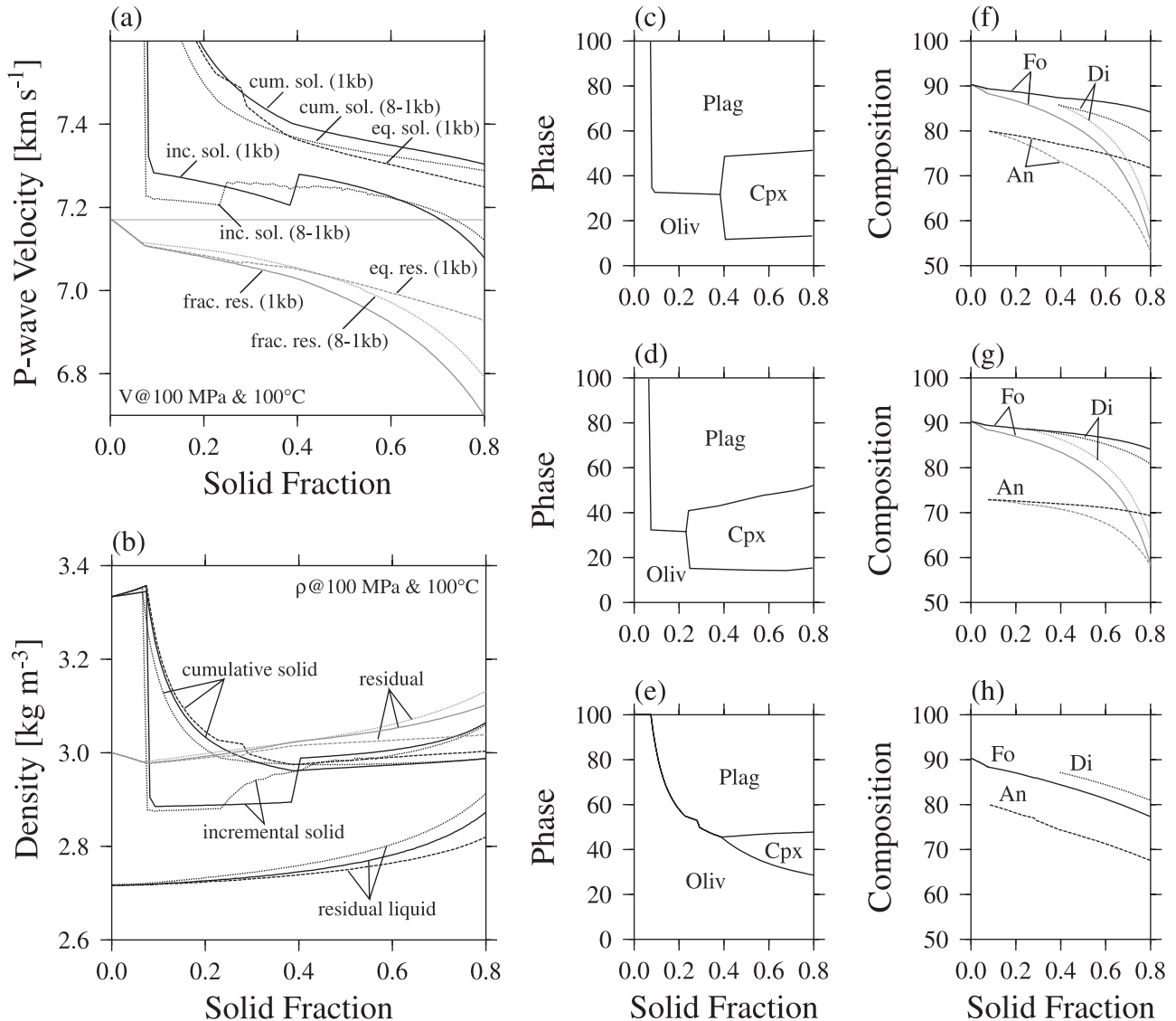
Figure 2. Example of crystal fractionation modeling. Starting liquid is polybaric near-fractional melt aggregated from a triangular shaped melting regime, with mean melt fraction of 9% and mean pressure of melting of 1.5 GPa, as calculated by *Kinzler* [1997] (SiO_2, 48.2%; TiO_2, 0.94%; Al_2O_3, 16.4%; Cr_2O_3, 0.12%; FeO, 7.96%; MgO, 12.5%; CaO, 11.4%; K_2O, 0.07%; Na_2O, 2.27%). Three fractionation paths are considered: (1) fractional crystallization at 100 MPa (solid), (2) equilibrium crystallization at 100 MPa (dashed), and (3) polybaric fractional crystallization at 800 to 100 MPa (dotted). (a) *P* wave velocities of cumulative fractionating assemblage and norm-based assemblage for residual liquid phase are calculated at a pressure of 100 MPa and a temperature of 100°C (note that this is different from the reference state defined in this paper) and shown as black and gray lines, respectively. Velocity of incremental fractionating assemblage is also shown as a thin gray line for fractional crystallization cases. (b) Solid densities are calculated at the same reference state. Residual liquid densities of residual phases are also shown. Phase proportions and compositions of fractionating assemblage are shown in Figures 2c–2h: (c, f) fractional crystallization at 100 MPa, (d, g) polybaric fractional crystallization at 800–100 MPa, and (e, h) equilibrium crystallization at 100 MPa. Abbreviations are Oliv (olivine), Plag (plagioclase), Cpx (clinopyroxene), Fo (forsterite content), Di (diopside content), and An (anorthite content).

predict accurately norm-based velocity over a wide range of pressure and melt fraction, without introducing spurious oscillations due to higher polynomials. The W_L window captures the behavior at low *F* and *P* whereas the W_H window covers the behavior at high *F* and *P*. The parameters P_t and F_t, which control the transition between these two windows, were determined by trial and error and were not a part of linear regression.

[14] We note that mantle melts of *Hirose and Kushiro* [1993] are not used in this regression. The calculation of melt fraction by *Hirose and Kushiro* [1993] is based on the Na_2O concentration in melt, which could lead to an over-
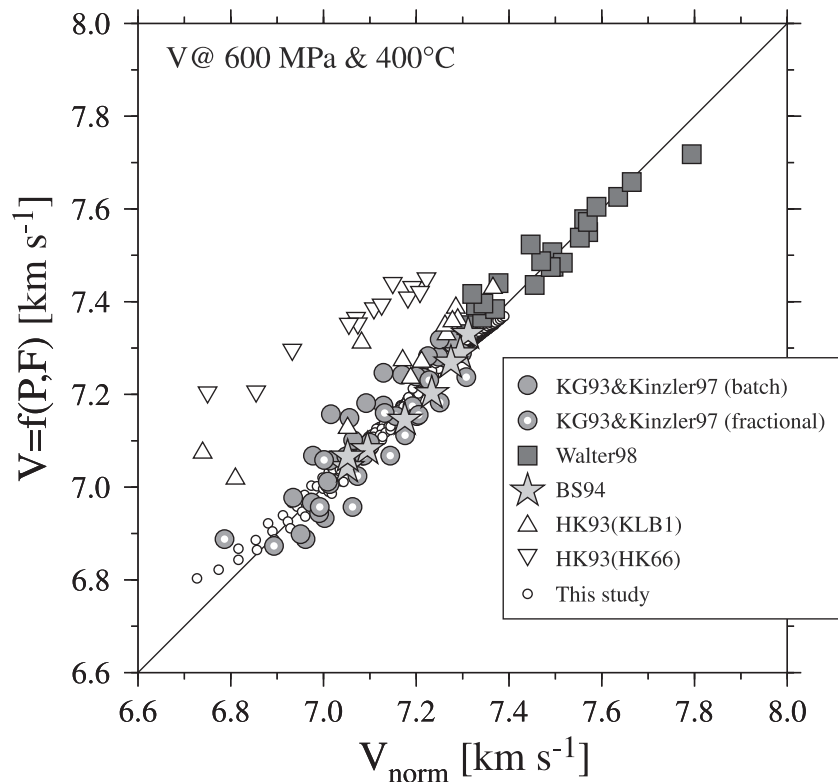
Figure 3. Relationship of norm-based *P* wave velocity to predicted *P* wave velocity based on pressure and fraction of melting (equation (1)), for experimental and calculated liquids for the melting of mantle lherzolite [*Kinzler and Grove*, 1992; *Hirose and Kushiro*, 1993; *Kinzler and Grove*, 1993; *Baker and Stolper*, 1994; *Kinzler*, 1997; *Walter*, 1998]. Small circles denote isobaric batch melts supplemented by us using the method of *Kinzler* [1997]. The mantle melts of *Hirose and Kushiro* [1993] are excluded from linear regression. One standard deviation is 0.01 km s^{-1} for the supplementary melt data and 0.05 km s^{-1} for the published melt data. Gray circles with dots denote polybaric fractional melts calculated by *Kinzler and Grove* [1993] and *Kinzler* [1997]. Predicted velocities for HK66 melts using equation (1) are systematically higher than their norm-based velocities, mainly because the melting of HK66, a pyroxenite, is associated with much higher degrees of melting compared to the melting of peridotites.

estimate [e.g., *Kogiso et al.*, 1998]. In addition, half of the Hirose and Kushiro melting data are on a pyroxenite, HK66, which is significantly different from pyrolite. All other data are for melting of mantle peridotites similar to "pyrolite" [e.g., *Ringwood*, 1975; *Hart and Zindler*, 1986; *McDonough and Sun*, 1995], with minor differences in composition. One standard deviation of this regression is about 0.01 km s^{-1} for the calculated supplementary data and about 0.05 km s^{-1} for the experimental data. Though the number of the supplementary data is an order of magnitude larger than that of the published data, we found that equal weighting of supplementary and experimental data for linear regression (in terms of individual weighted misfits) is optimal to minimize both misfits. The uncertainty of 0.05 km s^{-1} is probably due to a nonlinear, second-order relation between norm-based velocity and the mantle melting parameters, variation in source composition (the spread of whole rock Mg#s of mantle peridotites in the cited studies is 1.3%), and the difference of melting styles (i.e., batch in experiments and fractional for calculated melts).

[15] The majority of melt data used here are from batch melting experiments, and others are calculated, aggregated melts from polybaric fractional melting, modeled by *Kinzler and Groove* [1992] and *Kinzler* [1997]. For the latter, we used the mean pressure and degree of melting for the aggregate melts in the linear regression, and Figure 3 suggests that at least in terms of norm-based bulk crustal velocity, the difference in melting styles is only of minor importance. Because the importance of near-fractional melting in the generation of mid-ocean ridge basalts (MORB) is clear from geochemical evidence [e.g., *Klein and Langmuir*, 1987; *Johnson et al.*, 1990; *Sobolev and Shimizu*, 1993] as well as physical arguments [e.g., *McKenzie*, 1984; *Daines and Richter*, 1988], this weak sensitivity of bulk velocity to melting styles is particularly encouraging for our approach, which relies heavily on batch melting experiments. The actual melting style is probably somewhere between pure batch and pure fractional modes, owing to likely melt-rock reaction associated with melt migration [e.g., *Kelemen et al.*, 1995; *Lundstrom et al.*, 1995; *Kelemen et al.*, 1997a], further reducing the possible importance of fractional melting in our interpretation of crustal velocity.

[16] This empirical relation between norm-based bulk crustal velocity and mantle melting parameters such as *P* and *F* will be used later to calculate the crustal manifestation
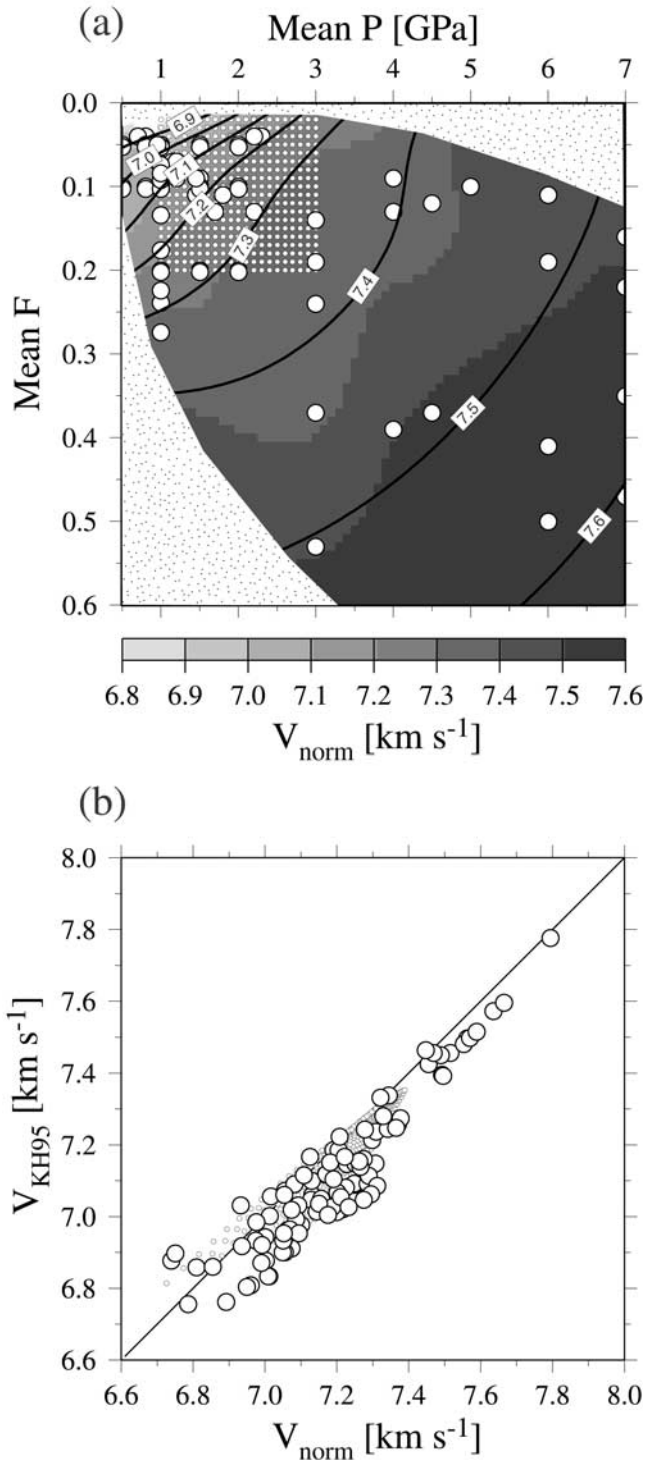
Figure 4. (a) Mantle melt data used for regression (shown as large open circles for published melts and small circles for our supplementary melts) are gridded as a function of the pressure and fraction of melting, and contours of predicted velocity based on our new regression are overlaid as solid lines. (b) Comparison of norm-based velocity with velocity calculated using equation (3).

of various mantle melting processes. A similar form of empirical relation was derived by KH95 as

$$V_p^{KH95} = 6.712 + 0.16P + 0.661F \qquad (2)$$

at the reference state of 600 MPa and 400°C. These two equations indicate different relations between norm-based bulk crustal velocity and the pressure and degree of melting (Figure 4a), and the possible causes of this discrepancy need to be clarified. First of all, our regression is based on an expanded data set of mantle melt compositions, including higher-pressure data of *Kinzler* [1997] and *Walter* [1998], as well as our calculated, isobaric batch melts. A more important difference, however, lies in the method of assigning velocity to melt composition. Compiling the laboratory measurements of the velocities and compositions of igneous and metamorphic rocks, KH95 derived the following empirical relation,

$$V_p^{KH95} = 7.854 - 0.024wt\%SiO_2 + 0.029wt\%MgO \qquad (3)$$

for the reference state. One standard deviation of this regression is 0.19 km s^{-1}, and adding additional oxides did not significantly improve the fit. Though the regression for equation (2) itself has a standard deviation of only 0.02 km s^{-1}, the large error of equation (3) essentially determines the prediction error of equation (2). There are several possibilities to explain the large standard deviation of equation (3); (1) laboratory measurements may sometimes suffer from residual porosity, (2) alteration introduces secondary mineral phases that are not present in pristine igneous crust, and (3) chemical analyses and velocity measurements are often conducted on different samples from the same rock, so that local heterogeneity in mineralogy and texture may obscure the relation between velocity and composition [e.g., *Jackson et al.*, 1990]. Figure 4b compares the velocities predicted by the equation for mantle melts with their norm-based velocities. Compared to our method, equation (3) systematically underpredicts velocity, suggesting that some bias in the composition-velocity relation was introduced in the equation through the approach based on published laboratory data.

[17] Compared to the KH95 approach, our new equation (1) is more sensitive to melt fraction and less sensitive to the pressure of melting (Figure 5 of KH95 and Figure 4a). In particular, for a melting condition that is believed to be appropriate for the generation of normal MORB (i.e., mean pressure of melting of 1 GPa and mean melt fraction of 0.1), our equation predicts bulk crustal velocity of 7.1 km s^{-1}, whereas the equation of KH95 predicts 6.95 km s^{-1}. Though the latter value is closer to the global average of oceanic lower crustal velocity [e.g., *White et al.*, 1992], this coincidence is perhaps fortuitous. The majority of oceanic lower crust may be affected by crack porosity, so this sort of direct comparison may not be valid. We discuss this issue further in section 3.

2.3. Theoretical Upper and Lower Crustal Velocities

[18] We modeled perfect fractional crystallization for all the published mantle melt data, at pressures of 100, 400, and 800 MPa. We denote the velocity of the cumulative fractionated assemblage as theoretical lower crustal velocity. The deviation of the theoretical lower crustal velocity from the
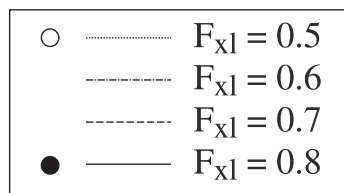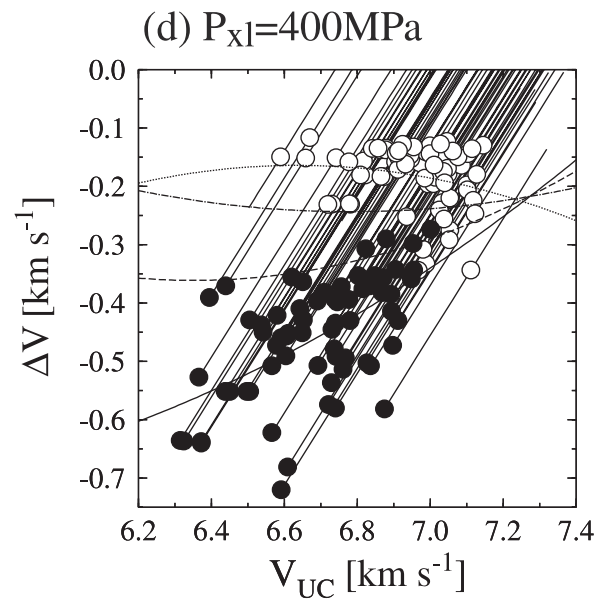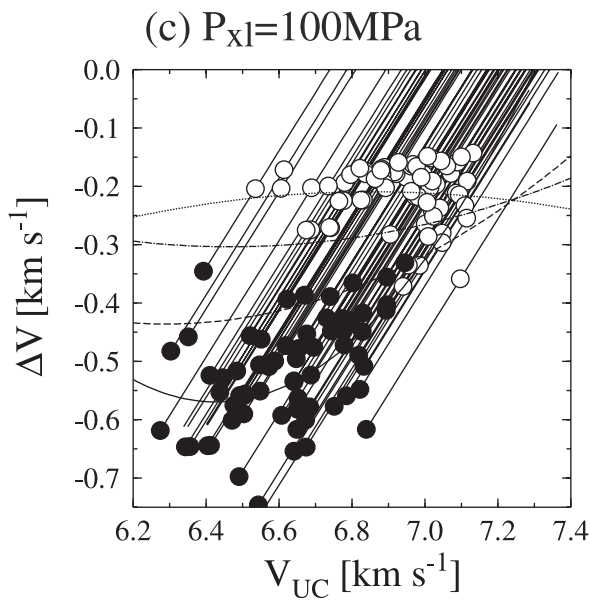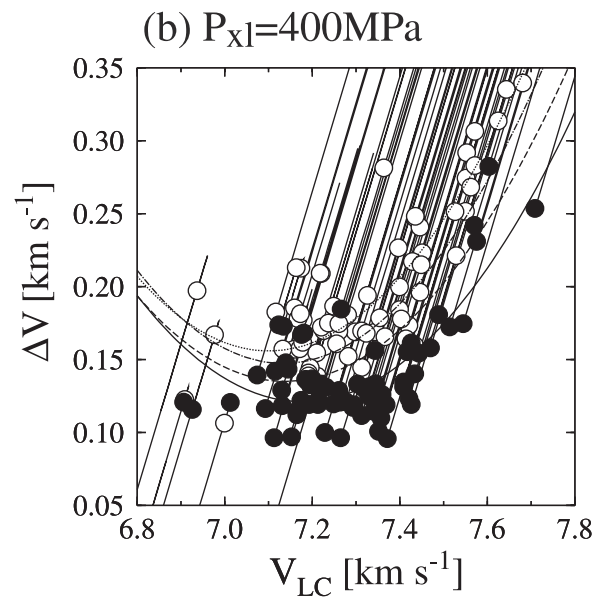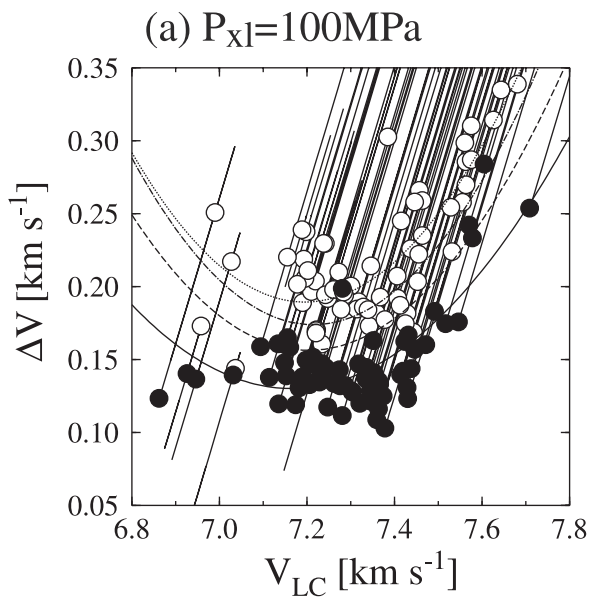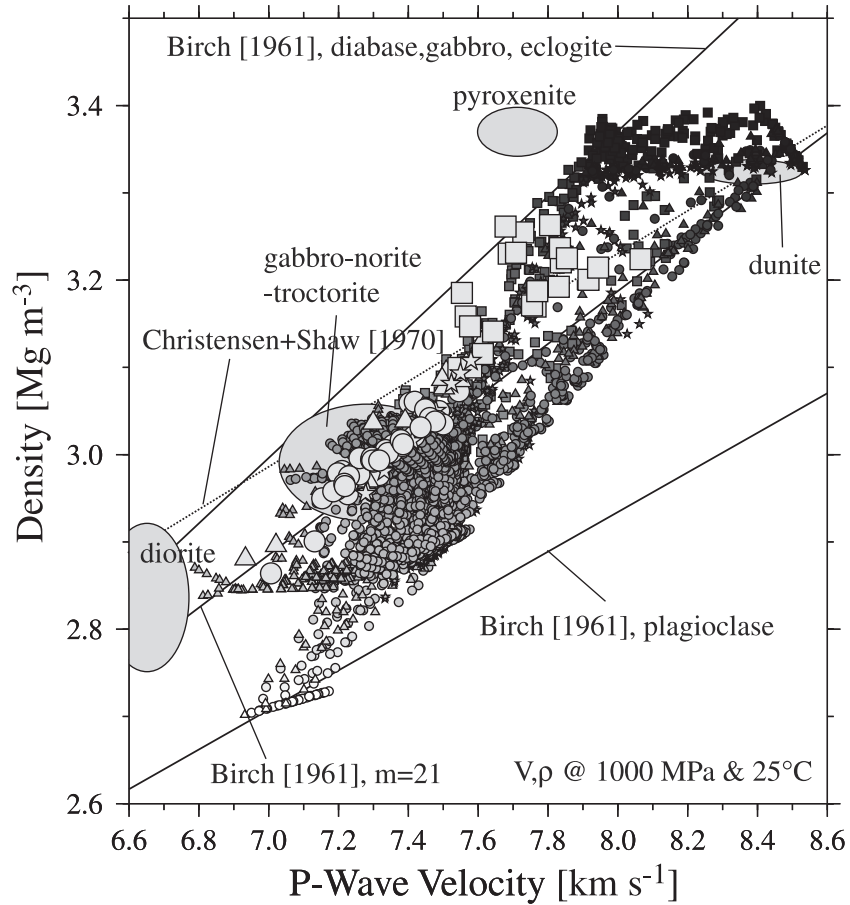
Figure 6. Covariation of P wave velocity and density of mafic and ultramafic rocks at 1000 MPa and 25°C. Large symbols denote norm-based calculations for mantle melts, and small symbols denote fractionated crystal assemblages formed at a range of crustal pressures (100–800 MPa). Ellipses denote laboratory data for diorite, gabbro-norite-troctorite, pyroxenite, and dunite, reported by *Christensen and Mooney* [1995]. Three solid lines are taken from *Birch* [1961] for plagioclase, rocks with mean atomic weight of ∼21, and diabase-gabbro-eclogite. Dotted line is for normal oceanic crust based on samples dredged from the Mid-Atlantic Ridge [*Christensen and Shaw*, 1970].

norm-based bulk crustal velocity is summarized in Figure 5. Subtracting this deviation from the *observed* lower crustal velocity provides a lower bound on the possible range of bulk crustal velocity, for a given average lower crustal velocity with the corresponding proportion of lower crust. For a lower crustal fraction of 0.5, for example, the norm-based bulk crustal velocity can be lower than the observed lower crustal velocity by 0.20 km s^{-1} at most. This bound is highly variable for low solid fractions, illustrating the strong dependence of each specific crystallization path on starting melt composition. As the solid fraction increases, however, the bound and its scatter both decrease gradually (Figure 5). The difference converges to zero at complete solidification. At solid fractions of 0.7–0.8, the deviation is about 0.15 km s^{-1} with a standard error of 0.02 km s^{-1} for a typical range of crustal velocities, nearly independent of crystallization pressures (Figures 5a and 5b).

[19] Similarly, the norm-based velocity for a residual liquid composition is denoted as the theoretical upper crustal velocity, and its difference from bulk crustal velocity

Figure 5. (opposite) Effects of fractional crystallization on P wave velocities of fractionating solid phase and residual liquid phase. (a) P wave velocity of cumulative fractionating phases (denoted V_{LC}) is plotted versus deviation of P wave velocities from bulk crustal velocity, for the fractionation paths at a crystallization pressure of 100 MPa of all the experimental mantle melts in our database (thin line). Velocities are values at 600 MPa and 400C. Open and solid circles denote the loci of fractionation paths at solid fractions of 0.5 and 0.8, respectively. To quantify the scatter for a given solid fraction, quadratic regressions are made at solid fractions of 0.5 to 0.8, and one standard deviation gradually decreases from 0.03 ($F_{xl} = 0.5$) to 0.02 ($F_{xl} = 0.8$). (b) Same as Figure 5a but at a crystallization pressure of 400 MPa. (c) Same as Figure 5a but with P wave velocity of rocks formed via equilibrium crystallization of the residual liquid phase (V_{UC}) and its deviation from bulk crustal velocity. One standard deviation of quadratic regression increases from 0.06 ($F_{xl} = 0.5$) to 0.09 ($F_{xl} = 0.8$). (d) Same as Figure 5c but at a crystallization pressure of 400 MPa. Similar results are obtained for a crystallization pressure of 800 MPa.
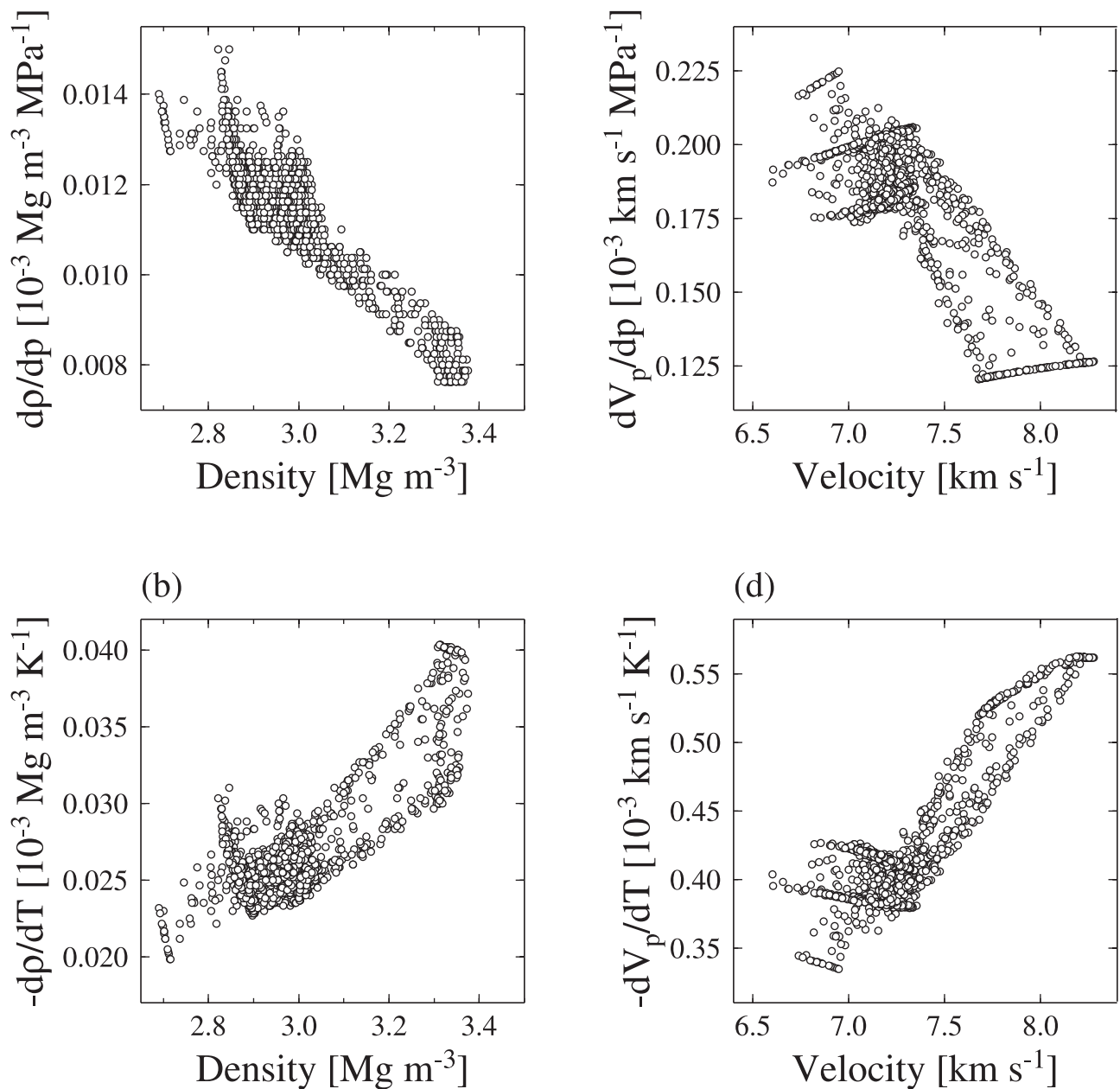
(b)

(d)

Figure 7. Theoretical pressure and temperature derivatives for density and velocity, calculated at 600 MPa and 400°C, using fractionated crystal assemblages formed at a range of crustal pressures (100–800 MPa).

is also shown in Figure 5. Though this velocity could never be observed because of high porosity and variable degrees of alteration in actual upper crust, we note that there are a wide range of possible upper crustal velocities (6.3–7.3 km s^{-1}). The deviation shows greater scatter as a solid fraction increases, implying that it is impractical to try to estimate hypothetical bulk crustal velocity using the composition of an evolved lava with reasonable accuracy. This observation motivates the strategy of using lower crustal velocity as the most practical approach to extract compositional information from crustal velocity structure.

2.4. Velocity-Density Systematics

[20] One of the benefits of the crystallization modeling described above is that we can also construct theoretical velocity-density systematics for pristine igneous rocks, with temperature and pressure derivatives. The compressional wave velocities and densities of fractionated assemblages, at a pressure of 1 GPa and a temperature of 25°C, are plotted in Figure 6, together with those for parental melt compositions. The reference state used here is chosen so as to facilitate comparisons with published empirical relations based on laboratory data.

[21] For each crystal assemblage, we can calculate its velocity and density at any given temperature and pressure, using the temperature and pressure derivatives of constituent minerals. Theoretical temperature and pressure derivatives for crystal assemblages can thus be calculated using finite difference approximation (Figure 7). The nonlinear effect of mixing is clearly seen, but the overall behavior can
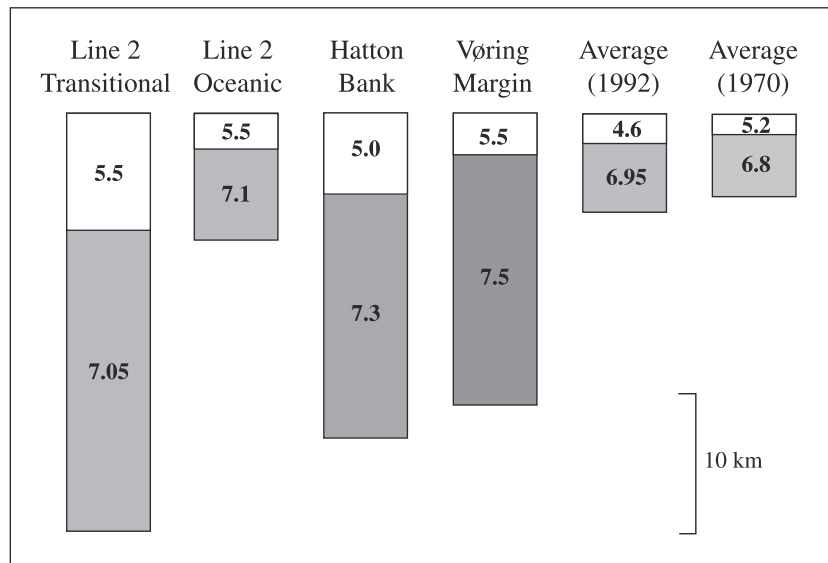
Figure 8. Two-layer *P* wave velocity models (upper and lower crust) for North Atlantic margins and normal oceanic crust. From left to right, transition zone and oceanic crust from SIGMA transect 2 (southeast Greenland margin; Figure 14c), Hatton Bank transition zone crust [*Fowler et al.*, 1989], Vøring Margin transition zone crust [*Zehnder et al.*, 1990], global average of normal oceanic crust compiled by *White et al.* [1992] and *Shor et al.* [1970].

be well approximated with linear relationships, which are useful in correcting observed velocities at various temperatures and pressures to the reference state. The calculated derivatives for velocity are qualitatively similar to those based on laboratory measurements of mafic and ultramafic rocks [e.g., *Christensen*, 1979; *Kern and Tubia*, 1993], but this theoretical confirmation, based on single crystal data and mixture theories, is important because the laboratory determination of pressure and temperature derivatives may be affected by residual porosity and hysteresis in crack closure, both of which are insignificant at geologic time scales [*Christensen*, 1974, 1979]. In addition, the virtue of our theoretical velocity-density data is that we can comprehensively explore possible regions in the *V*-ρ space for pristine igneous rocks originating from mantle melting. The mapping of this permissible space is particularly useful when velocity structure is used to infer possible density structure to study gravity anomalies [e.g., *Korenaga et al.*, 2001].

3. Bulk Crustal Velocity of Normal Oceanic Crust

[22] To interpret the velocity structure of "abnormal" igneous crust constituting LIPs, a proper understanding of the seismic velocity of normal oceanic crust is essential. The lower crustal velocity of normal oceanic crust with a thickness of 6–7 km has been observed to be around 6.9 km s^{-1} worldwide [e.g., *Raitt*, 1963; *Shor et al.*, 1970; *White et al.*, 1992] (Figure 8). Crustal velocities exceeding this value have been commonly interpreted as an indication of anomalous crustal composition. *White and McKenzie* [1989] were the first to attempt to quantitatively infer mantle melt compositions from the velocity of igneous crust. On the basis of the melting model of *McKenzie and Bickle* [1988], they predicted bulk crustal velocities of 6.9 to 7.2 km s^{-1} as the possible outcome of the melting of mantle with potential

temperatures (i.e., hypothetical temperature of mantle adiabatically brought to the surface without melting) of 1280–1580°C. In the framework of *McKenzie and Bickle* [1988], passive upwelling of mantle with a potential temperature of 1280°C results in the formation of normal oceanic crust, and velocities higher than 6.9 km s^{-1} are interpreted as the result of unusually high potential temperatures.

[23] The assumption that the melting of normal mantle should result in bulk crustal velocity of around 6.9 km s^{-1} was also adopted by KH95, and their interpretation of a high bulk crustal velocity of 7.3 km s^{-1} observed in thick igneous crust of the U.S. East Coast was primarily based on its deviation from the "normal" crustal velocity of 6.9 km s^{-1}. On the other hand, *Zehnder et al.* [1990] interpreted a lower crustal velocity of as high as 7.5 km s^{-1}, observed at the Vøring margin, as the result of the melting of normal mantle (but with active upwelling to generate thick crust), based on the similarity of Vøring lower crustal velocities to laboratory measurements of velocities of gabbroic rocks sampled from ophiolites. For the group working on the Vøring data, the large thickness of igneous crust, combined with lower crustal velocities that were "similar" to those for normal oceanic crust, was interpreted as evidence for active upwelling of normal mantle during the opening of the North Atlantic by *Mutter et al.* [1988], as opposed to passive upwelling of hot mantle in the plume head hypothesis presented by *White and McKenzie* [1989]. Thus it appears that there has been no consensus among marine seismologists on the seismic velocity of igneous crust resulting from the melting of mantle with normal potential temperature.

[24] It is known from laboratory studies that the compressional wave velocity of gabbroic rocks at the pressure and temperature of normal oceanic lower crust is generally higher than 7.0 km s^{-1} [e.g., *Christensen and Salisbury*, 1975; *Spudich and Orcutt*, 1980]. The example of crystal-

lization modeling presented in Figure 2, which used a potential primary melt composition for normal MORB as a starting liquid, also suggests that the norm-based bulk crustal velocity for normal MORB could be higher than 7.1 km s^{-1}. The fractional cumulative assemblages have velocities higher than 7.3 km s^{-1}, comparable to laboratory data for relatively unaltered mafic cumulates sampled from ophiolites [e.g., *Christensen and Smewing*, 1981].

[25] Hydrothermal alteration may be influential in reducing observed, oceanic lower crustal velocity compared to our calculated values for pristine igneous rocks, and to laboratory measurements on one inch cylinders of lower crustal samples. A number of petrological and geochemical studies of lower crust from ophiolites [e.g., *Gregory and Taylor*, 1981; *Pallister and Hopson*, 1981] and drilled samples of oceanic crust [e.g., *Dick et al.*, 1991; *Manning and Macleod*, 1996] indicate some hydrothermal alteration, and the lower crustal velocity of 6.9 km s^{-1} was once thought to reflect the dominant presence of hornblende metagabbro [*Christensen and Salisbury*, 1975].

[26] Field evidence from the Oman ophiolite and from ODP drill core, however, suggests that hydrothermal alteration is localized within cracks and veins, and that the majority of the cumulate lower crust is relatively unaltered with less than a few percent hornblende [e.g., *Gregory and Taylor*, 1981]. This low degree of alteration is not sufficient to reduce the velocity of gabbroic rocks to 6.9 km s^{-1} (Figure 9a). A more likely explanation is residual crack porosity, created by hydrothermal circulation and/or thermal contraction. Figure 9b shows that if pore aspect ratio is low (i.e., more crack-like), porosity as low as 0.5% can significantly lower velocity. Oceanic gabbroic rocks recovered by drilling exhibit a broad correlation between velocity and porosity [*Iturrino et al.*, 1991, 1996], which is consistent with the trend calculated for low aspect ratio porosity. We note that while reported porosities for these gabbroic rocks were measured at atmospheric pressure, the corresponding velocities shown in Figure 9b were measured at a pressure of 200 MPa. The observed correlation between porosity and velocity, therefore, suggests that residual porosity may remain open even at a typical Moho pressure for "normal" oceanic crust. To confirm that residual porosity is indeed the main cause of this correlation, we compare the measured velocity with norm-based velocity calculated from the whole rock composition of drill core (Figure 9b). For about one third of samples analyzed by *Iturrino et al.* [1991, 1996], we were able to find corresponding whole rock compositions reported by *Robinson et al.* [1987] and *Gillis et al.* [1993]. Whereas both kinds of data correspond to the same core, their sampling intervals in the core are, unfortunately, different. Our comparison here thus may suffer from local heterogeneity in mineralogy. Though not conclusive because of this sampling offset as well as the paucity of data, the norm-based velocities appear to be uncorrelated with porosity, which indicates that the observed trend in the measured velocities is mainly controlled by porosity.

[27] Given this possible porosity effect, therefore, the global average of normal crustal velocity may not be a useful reference value in interpreting the seismic structure of thick igneous crust. It may sound counter-intuitive, but the bulk crustal velocity of igneous crust formed by normal mantle melting does not have to be equal to the seismic velocity of normal oceanic crust. Thus, in this paper we rely instead on the calculation of norm-based bulk crustal velocity directly from melt composition. Though it is reasonable to expect that porosity should decrease as total crustal thickness increases because of greater lithostatic pressure, we do not know quantitatively the amount of residual porosity we should expect for greater depths. To resolve this issue, it is important to constrain the penetration depth of hydrothermal circulation and thermal cracking [e.g., *Lister*, 1974, 1983] as well as the mechanisms of crack healing and their timescales. Future research efforts are much warranted.

4. Mantle Melting Model With Active Upwelling

[28] On the basis of the relation between bulk crustal velocity and the pressure and degree of mantle melting (equation (1)), a possible connection between mantle melting processes and resultant crustal structure can be made. We shall consider a simple 1-D steady state melting model, which includes the effects of preexisting lithosphere and active mantle upwelling (Figure 10). The following treatment may be too simple to describe realistic melting dynamics, but our primary interest is to illustrate the first-order influence of three main parameters on mantle melting during the formation of LIPs: the mantle potential temperature, the thickness of a lithospheric lid, and the rate of active mantle upwelling. The importance of mantle potential temperature has been widely recognized as the fundamental control on magmatism at mid-ocean ridges [e.g., *Klein and Langmuir*, 1987; *McKenzie and Bickle*, 1988; *Kinzler and Grove*, 1992; *Langmuir et al.*, 1992] as well as LIPs [e.g., *White and McKenzie*, 1989; *Coffin and Eldholm*, 1994; *White and McKenzie*, 1995]. A lithospheric lid such as preexisting continental lithosphere and cold oceanic lithosphere imposes an upper limit on the mantle melting zone [e.g., *Fram and Lesher*, 1993; *Kelemen and Holbrook*, 1995]. In addition, the mantle upwelling rate is not necessarily equal to the surface divergence rate, and it can be much higher than passive upwelling in the presence of either a mantle plume [e.g., *Ribe et al.*, 1995; *Ito et al.*, 1996], or small-scale convection in the upper mantle [*Mutter et al.*, 1988; *Keen and Boutilier*, 1995; *Boutilier and Keen*, 1999; *Korenaga and Jordan*, 2002]. In this and following sections, we assume the mantle source composition to be pyrolitic. This assumption will be discussed in section 6.3.

[29] Adiabatically upwelling mantle, if not too cold, eventually intersects its solidus and begins to melt. We adopt the following solidus of dry peridotite [*Takahashi and Kushiro*, 1983]:

$$T_0 = 1150 + 120 P_0, \tag{4}$$

where P_0 is the initial pressure of melting in GPa, and T_0 is the mantle temperature at the pressure in °C. Following *McKenzie and Bickle* [1988], we define the potential temperature, T_p, as

$$T_p = T_0 - 20 P_0. \tag{5}$$

Given the above solidus and mantle adiabat, the amount of melting can be determined using the heats of fusion and heat capacities of mantle materials and a relation between temperature above the solidus and the extent of melting.
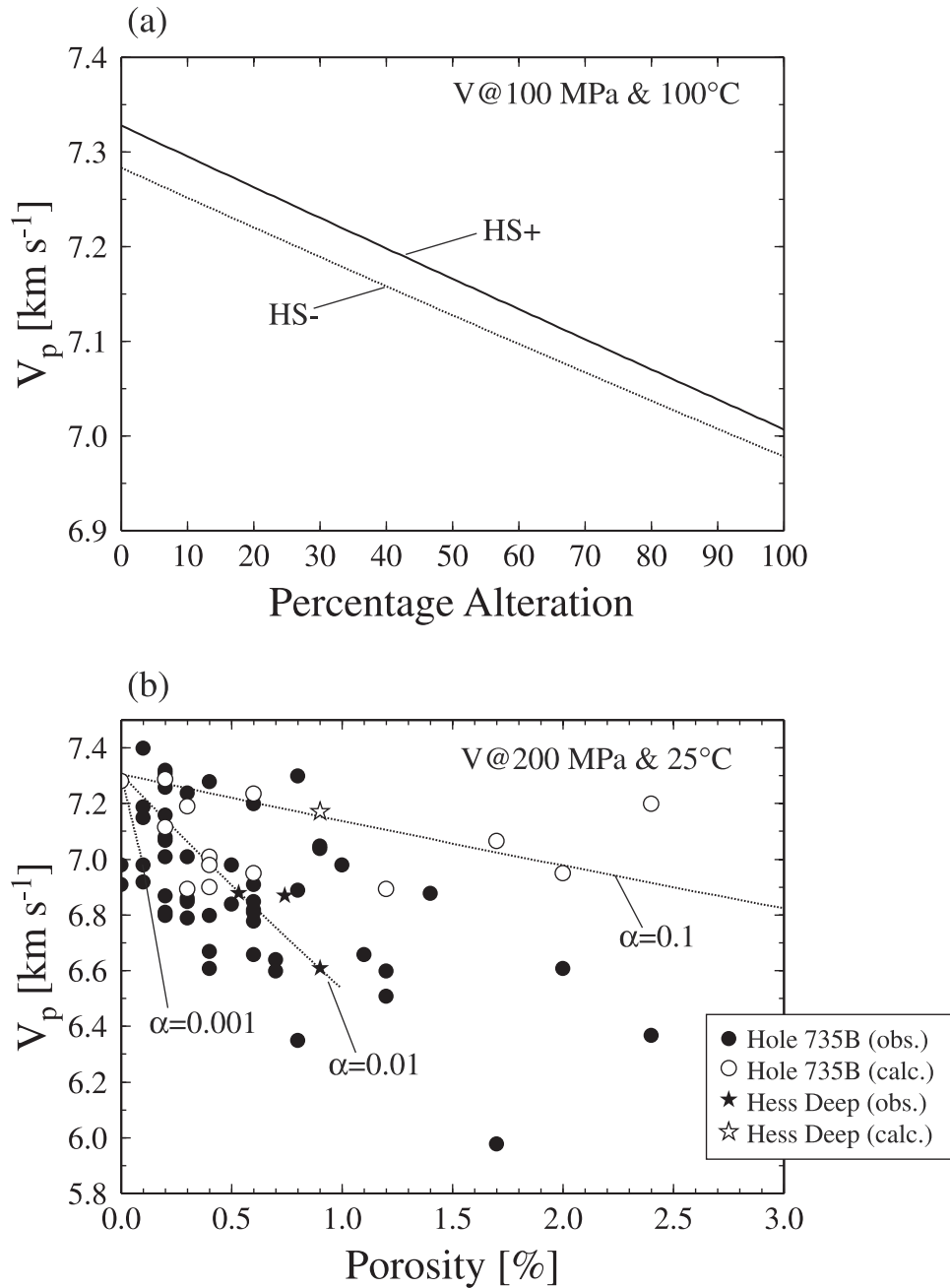
Figure 9. (a) Effect of hydrothermal alteration on gabbro velocity. Unaltered gabbro composition used here has 47% plagioclase (An60), 35% clinopyroxene (Di80), and 18% olivine (Fo75), which is the average of oceanic gabbroic rocks recovered from ODP Hole 735B, as reported by *Dick et al.* [1991]. We assume hydrothermal alteration simply results in the replacement of clinopyroxene with hornblende. Elastic moduli and density are first calculated for each mineral at 100 MPa and 100C, and Hashin-Shtrikman bounds (HS+ and HS−) for mineral assemblage are then calculated. (b) Effect of residual crack porosity on gabbro velocity. We first calculated effective elastic moduli of dry porous rock with different pore aspect ratios (0.1, 0.01, and 0.001) using the formula of *Kuster and Toksöz* [1974], and then applied the Gassmann low-frequency relations to obtain effective moduli for fluid saturated porous rock [e.g., *Mavko et al.*, 1998]. Elastic moduli for seawater are taken from *Wilkens et al.* [1991], and elastic moduli for pore-free gabbro are taken from the average of Hashin-Shtrikman bounds as calculated in Figure 9a. The results are shown as dotted lines. Also shown are velocity-porosity data for gabbroic rocks recovered from ODP Hole 735B (solid circle) [*Iturrino et al.*, 1991] and Hess Deep (solid star) [*Iturrino et al.*, 1996]. While porosity data are measured at atmospheric pressure, velocity data are measured at 200 MPa. Out of 58 samples analyzed by *Iturrino et al.* [1991, 1996], 17 samples have a reported whole rock composition [*Robinson et al.*, 1987; *Gillis et al.*, 1993], from which norm-based velocity is calculated (open circle is Hole 735B and open star is Hess Deep).
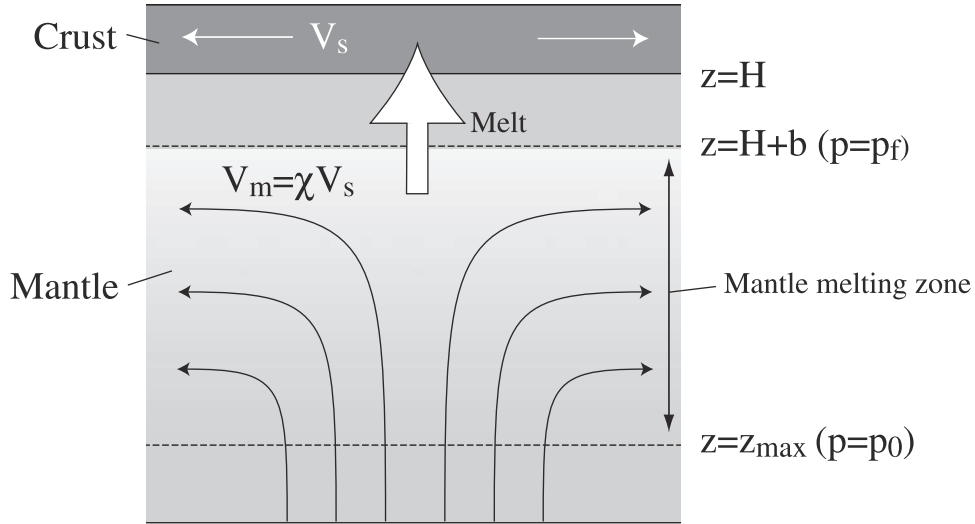
Figure 10. Schematic diagram of mantle melting model used in this study. Mantle upwelling rate (V_m) can be faster than surface divergence rate (V_s) by a factor of χ (active upwelling ratio). The mantle melting zone starts when the mantle adiabat intersects the solidus, and its upper limit is imposed by a lithospheric lid, which is composed of newly formed igneous crust (H), and preexisting lithosphere or cold oceanic mantle (b).

To first-order, melt fraction can be approximated as a linear function of pressure decrease from the initial pressure of melting as

$$F(P) = \left(\frac{\partial F}{\partial P}\right)_S (P_0 - P), \qquad (6)$$

where $(\partial F/\partial P)_S$ is a change in melt fraction with a change in pressure above the solidus during adiabatic decompression. This parameter is probably most important in relating the melting process to observable crustal thickness (melt volume), but its estimate varies from 10%/GPa to 20%/GPa [e.g., *Ahern and Turcotte*, 1979; *McKenzie*, 1984; *Langmuir et al.*, 1992; *Asimow et al.*, 1997]. Therefore we will test several choices for this parameter later in this section. The final pressure of melting is limited by a lithospheric lid, which includes newly formed igneous crust (H) and preexisting continental lithosphere or cold oceanic mantle (b),

$$P_f = (H + b)/30, \qquad (7)$$

in which we assumed 30 km GPa^{-1} for depth to pressure conversion. The mean fraction of melting is defined as,

$$\bar{F} = \frac{\int_{P_f}^{P_0} F(P)dP}{\int_{P_f}^{P_0} dP}. \qquad (8)$$

This is the bulk mean fraction of melting [*Plank et al.*, 1995]. For the linear melting function of equation (6), it reduces to $F = 0.5\, F(P_f)$. Similarly, the mean pressure of melting is defined as,

$$\bar{P} = \frac{\int_{P_f}^{P_0} PF(P)dP}{\int_{P_f}^{P_0} F(P)dP}. \qquad (9)$$

[30] For a triangular melting regime associated with mantle corner flow, the mean pressure of melting, assuming a linear melting function, is $(P_0 + 2P_f)/3$ for batch melting, and $(2P_0 + P_f)/3$ for fractional melting [*Langmuir et al.*, 1992], and more complex melting regimes would lead to different mean pressures [e.g., *Plank and Langmuir*, 1992]. A realistic mixing formula for mean melting pressure is probably somewhere between purely batch and purely fractional cases, especially for major element compositions [e.g., *Kelemen et al.*, 1997a], and we adopt $P = (P_0 + P_f)/2$ as a compromise. If all melt is emplaced as igneous crust, the crustal thickness is then calculated as,

$$H = 30\chi(P_0 - P_f)\bar{F}, \qquad (10)$$

where χ is the ratio of the mantle upwelling rate to the surface divergence rate. χ is ≥ 1, with χ of unity corresponding to passive upwelling. Another seismic observable, bulk crustal velocity, can be calculated from P and F, using equation (1). For given T_p, b, and χ, equations (6)–(10) can be solved in a closed form; the final pressure of melting can be expressed as,

$$P_f = P_0 + \frac{1}{\chi}\left(\frac{\partial F}{\partial P}\right)_S^{-1}\left\{1 - \left[1 + 2\chi\left(\frac{\partial F}{\partial P}\right)_S (P_0 - b/30)\right]^{\frac{1}{2}}\right\},$$
$$(11)$$

and the crustal thickness is then calculated using equation (10). For a more complex formulation of the melting function, however, the above equations must be solved numerically.

[31] Our definition of "active upwelling" is different from that which has been commonly used in the literature on mid-ocean ridge dynamics, so some clarification is necessary. Several authors have demonstrated that a decou-

pling of solid mantle flow from the surface divergence is possible when extra buoyancy due to high melt retention and lower Fe/Mg in residual solids is considered [e.g., *Rabinowicz et al.*, 1987; *Scott*, 1992; *Turcotte and Phipps Morgan*, 1992; *Su and Buck*, 1993; *Barnouin-Jha et al.*, 1997]. The resultant rapid solid upwelling is often referred as active mantle upwelling, and it has been suggested as a possible mechanism of melt focusing beneath mid-ocean ridges. In an extreme case in which all melts are retained, mantle melt would be at equilibrium at the shallowest pressure of melting; mean pressure of melting and mean melt fraction are simply the final pressure of melting and the maximum melt fraction, respectively, attained in the melting zone [*Langmuir et al.*, 1992]. Though this type of mantle dynamics associated with melting would add important complexity to the interpretation of igneous crustal structure, it depends on a number of assumptions on mantle rheology during melting, and we consider it still premature to incorporate its possible effects. Even without this type of active upwelling mechanism, however, the decoupling of mantle flow from the surface motion is still viable during the formation of LIPs. Since continental rifting is a transient process in which surface divergence evolves from null to some finite value, for example, mantle upwelling velocity due to a mantle plume, or to preexisting sublithospheric convection, can be significantly greater than that of plate-driven flow [e.g., *Korenaga and Jordan*, 2002]. The active upwelling ratio, χ, in our model is designated to quantify this decoupling as previously proposed by *Kelemen and Holbrook* [1995].

[32] Figure 11 shows some sample calculations based on our melting model, using a linear melting function with $(\partial F/\partial P)_S$ of 12%/GPa (standard model). The mean pressure of melting, the mean melt fraction, crustal thickness, and bulk crustal velocity are calculated as a function of mantle potential temperature, with a range of active upwelling ratio and preexisting lid thickness. A higher active upwelling ratio results in thicker crust, which in turn limits the melting zone, leading to slightly higher mean melting pressure and lower melt fraction (Figures 11a–11c). High pressure of melting and low melt fraction have competing effects on bulk crustal velocity, and they tend to cancel out (Figure 11d). A preexisting lid has similar but larger effects on melting pressure and melt fraction, and a reverse effect on crustal thickness (Figures 11e–11g). A thicker lid tends to lower the resultant crustal velocity (Figure 11h).

[33] There are of course an infinite number of other combinations of active upwelling ratio and lid thickness, but for the sake of discussion, we limit ourselves to two end-member cases: (1) active upwelling with zero lid thickness, and (2) non-zero lid thickness and passive upwelling. As shown in Figure 12a, these two cases can cover a considerable range of crustal thickness and velocity, and we think that more complicated cases should be considered only when some independent geological information requires them. The effect of a preexisting lid in the case of active upwelling, however, can easily be inferred from the case of passive upwelling; a thicker lid tends to reduce crustal thickness while maintaining crustal velocity. This crustal thickness and velocity (H-V_p) diagram concisely illustrates a possible relationship between seismic observables and mantle melting parameters.

[34] For comparison, we also construct a H-V_p diagram using the velocity equation of KH95 (Figure 12b). For given melting parameters, this diagram consistently predicts lower values for bulk crustal velocity. Another important difference is the effect of a lithospheric lid on crustal velocity. Whereas a thicker lid increases crustal velocity if we use the equation of KH95, such an effect is not predicted using our new equation (1). This may be counter-intuitive for some readers; because a lithospheric lid increases mean pressure of melting and decreases melt fraction of melting, resulting in lower SiO_2 and higher MgO contents in mantle melts, one might expect that a thicker lid should lead to higher crustal velocity. The reason for the lack of sensitivity to the lid effect with our new equation is that a thicker lid also increases Na_2O and FeO contents, thereby producing more albite and fayalite components, which have a low seismic velocity in crystalline rocks. Our approach with norm-based velocity takes into account this subtle balance of different compositional effects.

[35] To illustrate the sensitivity of the H-V_p diagram to the choice of a melting function, two more diagrams were made with (1) a linear function with a higher melting rate of 16%/GPa (Figure 13a), and (2) a three-stage melting function incorporating the effect of initial, small degrees of melting due to, e.g., H_2O and K_2O, and the effect of clinopyroxene exhaustion, similar to that calculated by *Asimow et al.* [1997] (Figure 13b). The overall features of all of these H-V_p diagrams, such as the location of passive upwelling curve and the effects of active upwelling and lithospheric lid, are very similar. The only critical difference is mantle potential temperature; for a given pair of crustal thickness and velocity, the estimate of mantle potential temperature would be systematically higher for a melting function with smaller $(\partial F/\partial P)_S$. Considering that our understanding of the mantle melting function is still limited, therefore, the actual value of potential temperature for a given H-V_p pair is highly uncertain. However, the inferred differences in potential temperature between areas with different H-V_p combinations - *but the same mantle melting function* - are more robust. In addition, estimates of active upwelling ratio or lid thickness should also be robust if bulk crustal velocity and crustal thickness are well determined.

5. An Example: Nature of Mantle Melting During the Formation of the Southeast Greenland Margin

[36] The 1996 SIGMA seismic experiment across the southeast Greenland margin employed dense receiver arrays and deep-penetrating air gun sources to provide deep-crustal seismic data of unprecedented quality on four transects (Figure 14a). Preliminary results for all four transects are summarized in *Holbrook et al.* [2001]. Following preliminary analysis, the transect 2 data were analyzed in more detail with joint refraction and reflection tomography to construct a P wave velocity model [*Korenaga et al.*, 2000]. A nonlinear Monte Carlo uncertainty analysis showed that the model was tightly constrained; the absolute uncertainty for vertically averaged velocity is less than 0.03 km s^{-1}. The interpretation of the velocity model based on the framework of KH95 suggested that the thick igneous crust observed in the continent-ocean transition zone was the result of active upwelling of mantle ($\chi > 8$) with almost
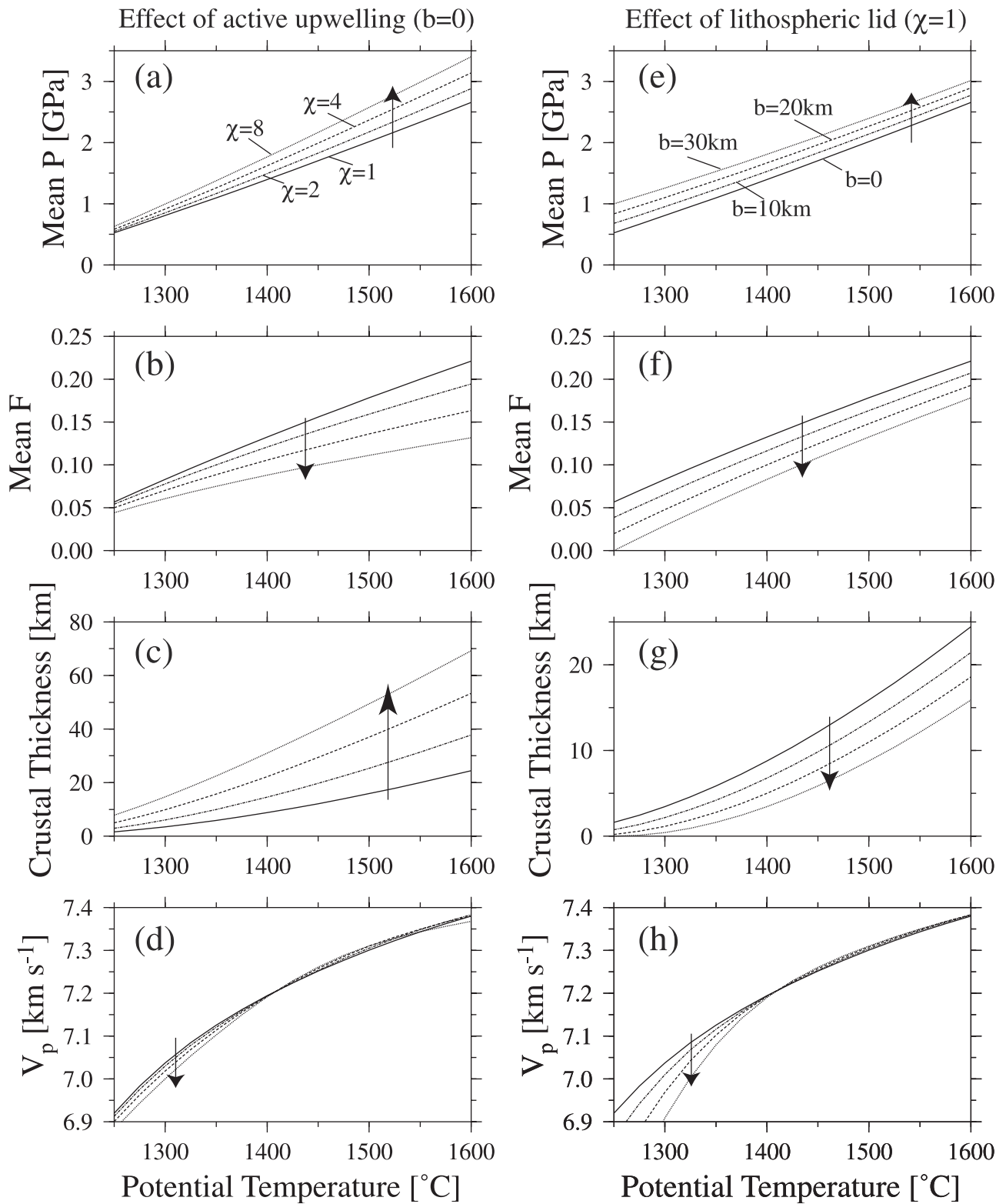
Figure 11. (a) Mean pressure of melting, (b) mean fraction of melting, (c) predicted crustal thickness, and (d) predicted bulk crustal velocity, are calculated as a function of mantle potential temperature, for several different active upwelling ratios and zero thickness of preexisting lid. A linear melting function with of 12%/GPa is used. (e)–(h) Similar calculations with different thicknesses of preexisting lid and passive upwelling.
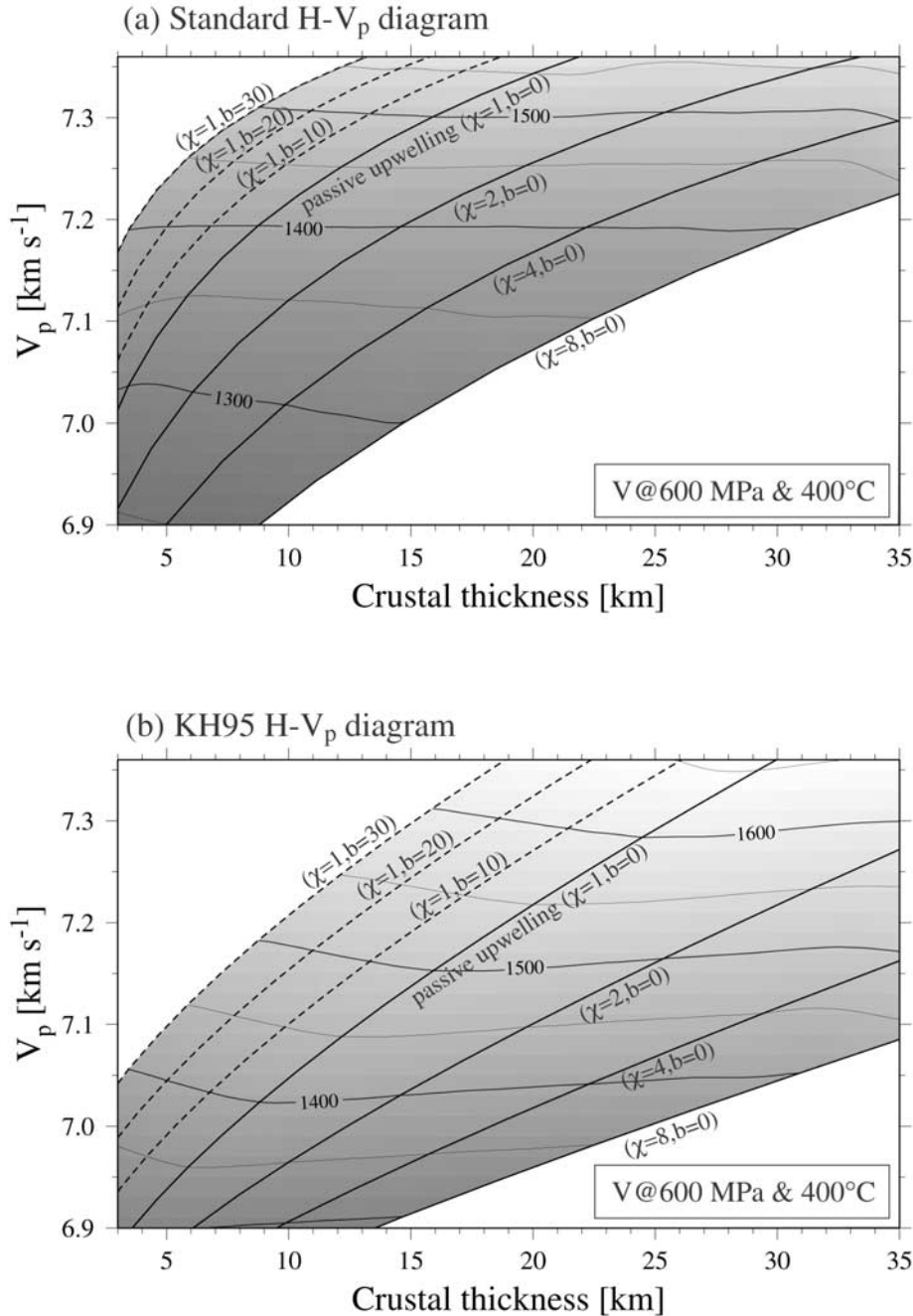
Figure 12. (a) Standard H-V_p diagram based on calculations presented in Figure 11. The contours of mantle potential temperature are drawn at 50C interval. (b) Same as Figure 12a but with the empirical relation of KH95 (equation (3)).

normal potential temperature. This interpretation, however, remained uncertain because the KH95 method involved other sources of uncertainty, such as the poorly constrained velocity-composition relationship and the assumption of uniform upper crustal velocity. In the example in this section, we reinterpret of the transect 2 velocity model.

[37] The thickness of the igneous crust on transect 2 varies from ~30 km in the continent-ocean transition zone to ~9 km in the deep-ocean basin near the seaward end (Figure 14b). The thickness of the upper crust, which is

marked by high velocity gradients, also changes along the transect, and the proportion of the upper crust is nearly constant at around 30% (Figure 15b). Despite its great thickness, the lower crust in the continent-ocean transition zone does not exhibit a notable increase in its velocity (Figures 14b and 14c), being conspicuously different from the thick, high velocity (>7.2 km s^{-1}) crust observed at the continent-ocean transition zone of other volcanic margins [e.g., *White et al.*, 1987; *Mutter and Zehnder*, 1988; *Holbrook and Keleman*, 1993] (Figure 8). After applying
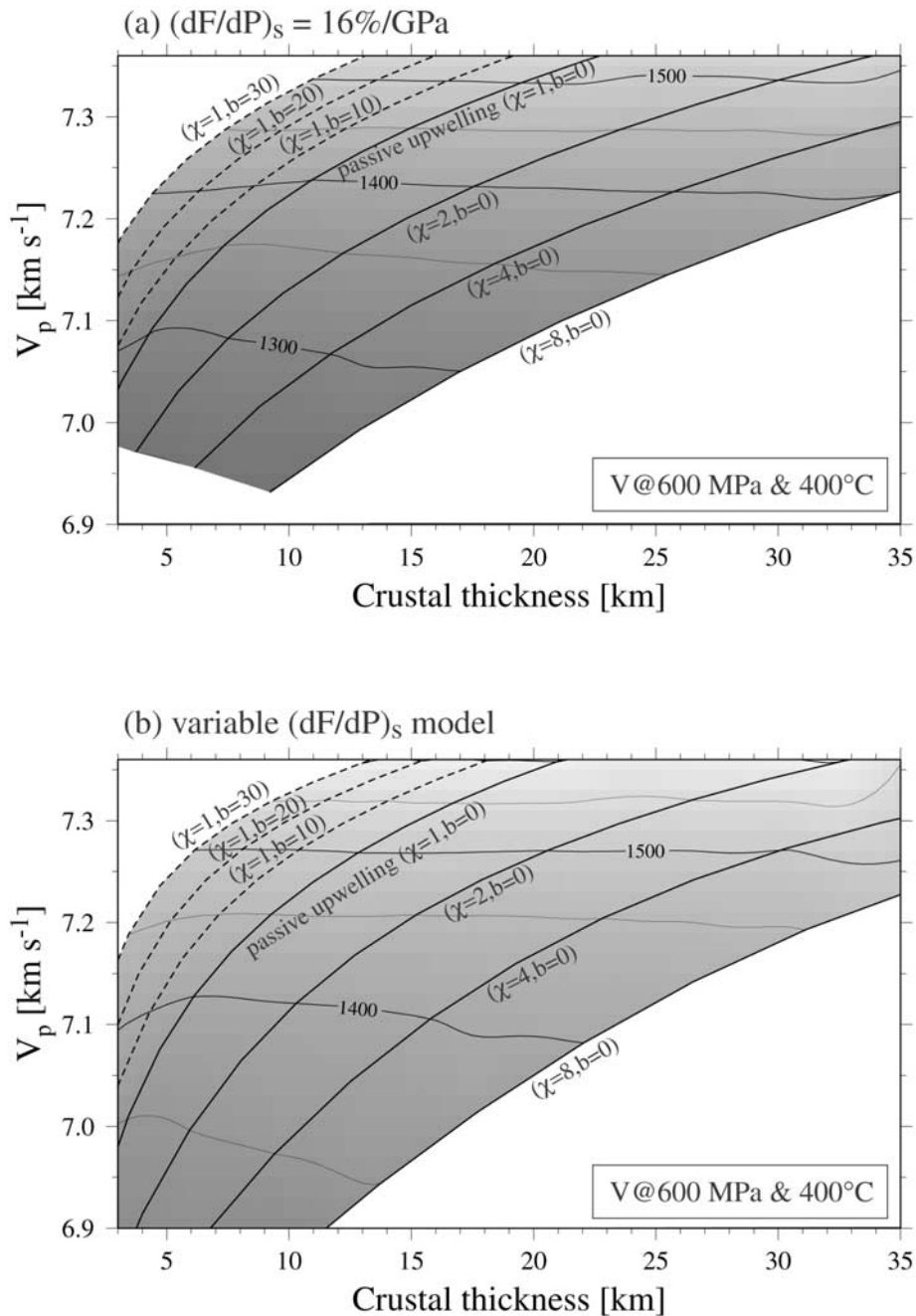
Figure 13. (a) Same as Figure 12a, but with of 16%/GPa. (b) Same as Figure 12a, but with a three-stage melting function to simulate the effects of low melt productivity at low melt fraction and of clinopyroxene exhaustion; $F_1 = 0.035dP$ ($dP < 1.15$ GPa), $F_2 = 0.23(dP - 1.15) + 0.04$ ($0.15 \leq dP < 0.175$ GPa), and $F_3 = 0.113(dP - 1.75) + 0.18$ ($dP \geq 1.75$ GPa), where dP denotes $P_o - P$. This is an approximation based on the results of thermodynamic calculations by *Asimow et al.* [1997].

a pressure correction of 0.2×10^{-3} km s^{-1} MPa^{-1} and a temperature correction of -0.4×10^{-3} km s^{-1} °C^{-1} (Figure 7), with respect to a reference pressure of 600 MPa and a reference temperature of 400°C, the harmonic mean of velocities is calculated for the igneous lower crust as a function of the model distance (Figure 15a). For the temperature correction, we assume a linear conductive geotherm with a thermal gradient of 20°C km^{-1} and a

surface temperature of 0°C. Velocities within a horizontal window of 20 km were averaged at each model distance, and we repeated this averaging procedure with 100 Monte Carlo ensembles to estimate uncertainty as in *Korenaga et al.* [2000].

[38] The average lower crustal velocity is plotted with the corresponding whole crustal thickness on the standard H-V_p diagram (Figure 15c). Note that the lower crustal velocity is
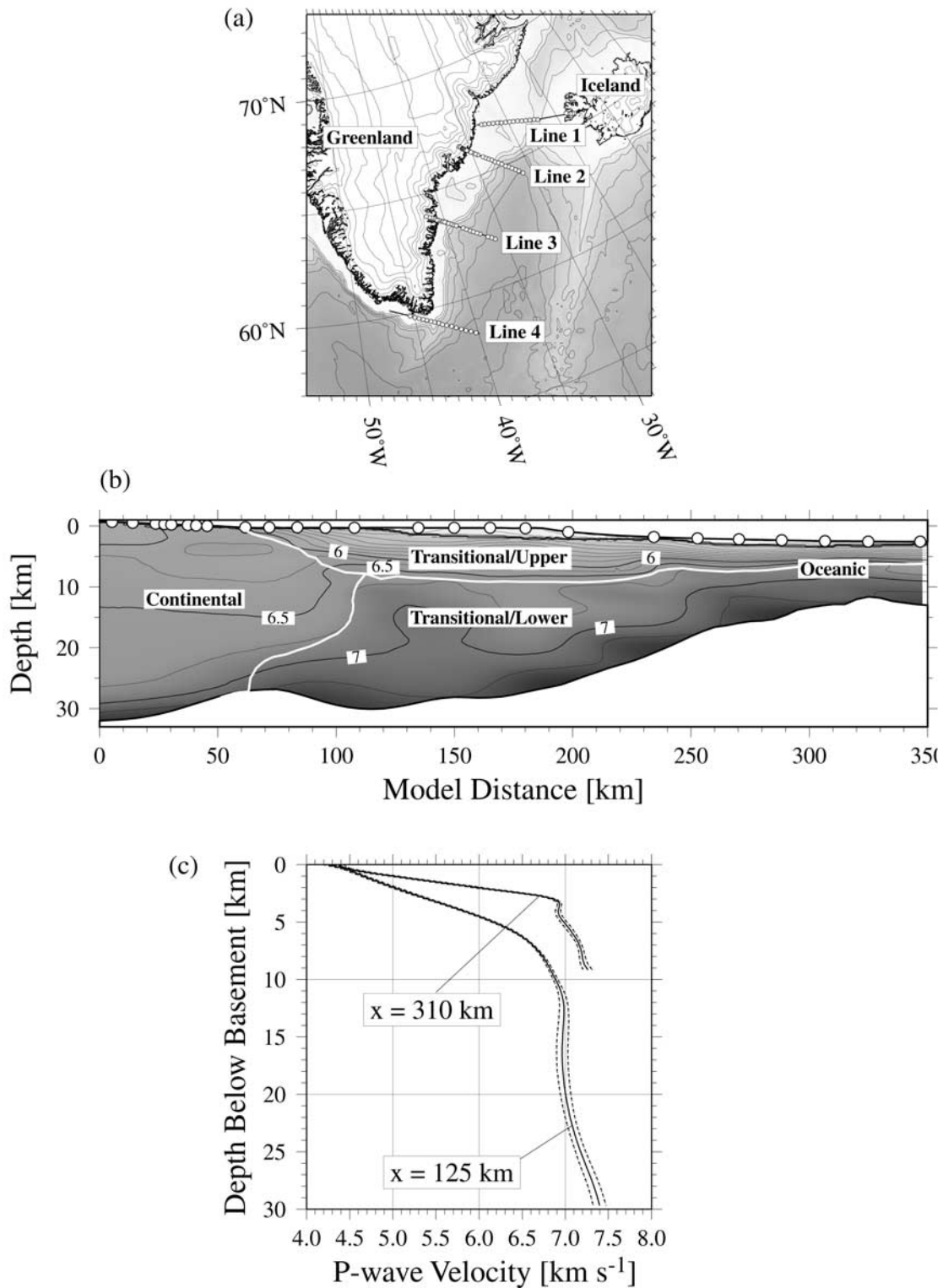
Figure 14. (a) Location of 1996 SIGMA transects. Open circles denote the location of seismic receivers, and solid lines denote shot lines. (b) *P* wave velocity model for transect 2 [after *Korenaga et al.*, 2000], with geological interpretation of continental, transition zone and oceanic crust. (c) 1-D velocity profiles sampled from Figure 14b at model distances of 125 km and 310 km. One standard deviation is shown as dashed, based on 100 Monte Carlo ensembles.
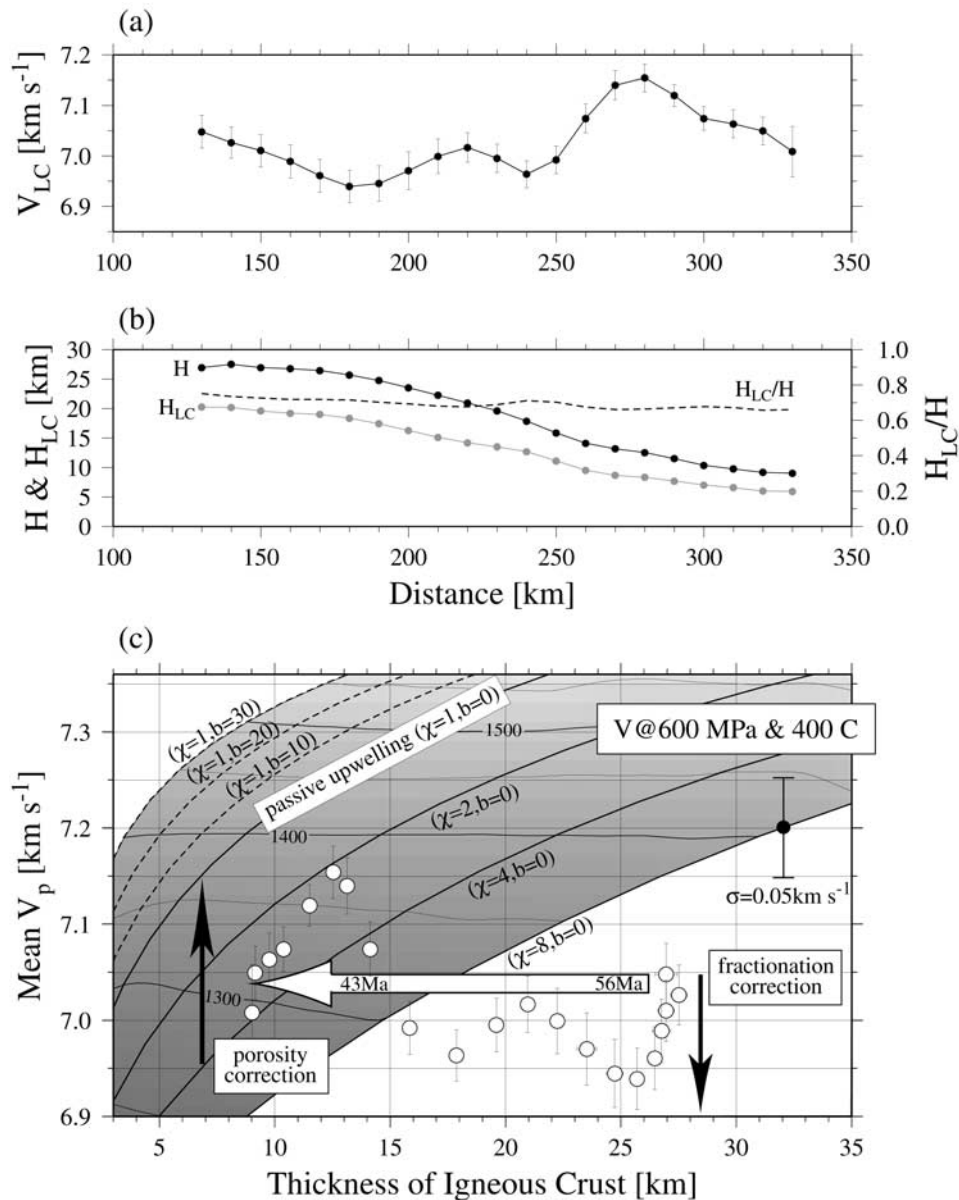
Figure 15. (a) Harmonic mean of the lower crustal velocity of SIGMA transect 2 is calculated at 10 km intervals with a 20 km wide averaging window, using 100 Monte Carlo ensembles. (b) Whole crustal (solid) and lower crustal (gray) thicknesses are calculated in a similar manner. Lower crustal fraction is also shown as dashed. (c) Mean velocity of the igneous lower crust is plotted as a function of corresponding whole crustal thickness (open circles with error bars), on the standard H-V_p diagram (Figure 12a).

the upper bound of the possible range of bulk crustal velocity. For a lower crustal proportion of ∼70% and a lower crustal velocity of ∼7.0 km s^{-1}, the bulk crustal velocity could be as low as 6.85 km s^{-1}, considering the maximum effect of fractionation (Figures 5a and 5b). For the thinner crust observed toward the seaward end, however, this upper bound is most likely invalid because an effect of crack porosity, lowering the lower crustal velocities, is expected. As described in a previous section, we thus focus on the thick (>15 km) crust, for which the correction for residual cracks may not be necessary. Furthermore, most of this thick crust is >100 km away from coastal dike swarm and >50 km away from our estimate of

the seaward end of continental crust. Fragments of stretched continental crust may be present in this zone, but it seems unlikely that they constitute a significant volume fraction. The H-V_p diagram suggests that an anomalously strong active upwelling of mantle (more than eight times faster than the surface divergence) is responsible for the formation of the thick igneous crust on transect 2. As already noted, the estimate of mantle potential temperature ranges from 1250–1350°C, depending on the choice of a melting function (Figures 12a and 13). However, in all cases the estimated potential temperature is not significantly higher than a normal potential temperature of ∼1300°C [e.g., *McKenzie and Bickle*, 1988; *Langmuir et al.*, 1992]. Though

the regression for equation (1), which is a key link between crustal velocity and mantle melting parameters, has a standard deviation of 0.05 km s^{-1}, vigorous mantle upwelling with almost normal temperature, as inferred by *Korenaga et al.* [2000], still seems to be a robust conclusion. This result is inconsistent with the thermal plume hypotheses proposed for the North Atlantic igneous province [e.g., *Richards et al.*, 1989; *White and McKenzie*, 1989; *Barton and White*, 1997], because a thermal plume is characterized by high mantle potential temperatures. Since the use of the H-V_p diagram would be more robust in comparison with adjacent seismic transects, the accurate determination of whole crustal velocity structure on all four SIGMA transects [*Holbrook et al.*, 2001] is essential to resolve outstanding questions on margin-wide mantle dynamics during the opening of the North Atlantic.

6. Discussion

[39] Utilizing the seismic structure of igneous crust to infer mantle dynamics has been repeatedly attempted in the past [e.g., *White and McKenzie*, 1989; *Kelemen and Holbrook*, 1995; *Farnetani et al.*, 1996; *Barton and White*, 1997], but previous studies suffer from one or more of the following flaws: (1) inaccurate and incomplete mantle melting model (lacking prediction of melt composition and consideration of active upwelling), (2) strong assumptions regarding crustal emplacement process, (3) poorly constrained calculation of bulk crustal velocity from melt composition, and (4) lack of robust uncertainty analysis for the crustal velocity model to be interpreted. This study addresses the first three; a way to resolve the fourth has already been presented elsewhere [*Korenaga et al.*, 2000]. We employ a bounding approach to connect lower crustal velocity to mantle melting parameters through theoretical bulk crustal velocity, without assuming any specific scenario for crustal accretion process. In the process of building this interpretation framework, we found that the lower crustal velocity of normal oceanic crust (~6.9 km s^{-1}) is hard to reconcile with primary MORB compositions unless the effect of crack porosity is considered. It is probably incorrect to use the crustal velocity of 6.9 km s^{-1} as a reference corresponding to normal mantle melting, and we can only utilize deep (>~8 km) lower crust where the effects of residual cracks are expected to be minimal.

[40] Our example for the southeast Greenland margin focused on the interpretation of thick lower crust. Our conclusion is significantly different from previous hypotheses about the formation of the North Atlantic igneous province. In deep crustal seismic studies, this igneous province is the best studied region in the past decade or so [*White et al.*, 1987; *Mutter and Zehnder*, 1988; *Fowler et al.*, 1989; *Morgan et al.*, 1989; *Zehnder et al.*, 1990; *Barton and White*, 1997], so further discussion of this discrepancy is needed. In this section, we first critically review the previous deep crustal studies of the North Atlantic continental margins, because the effect of velocity-depth ambiguity in seismic inverse problems may have been underestimated in the past. Then, we examine two major assumptions in our interpretation (and all previous interpretations): (1) all mantle melt is emplaced as seismically observable crust, and (2) the mantle source composition is

similar to pyrolite [e.g., *Ringwood*, 1975; *Hart and Zindler*, 1986; *McDonough and Sun*, 1995]. The validity of these two fundamental assumptions are discussed in order.

6.1. Previous Deep-Crustal Studies of the North Atlantic Margins

[41] As emphasized by KH95 and *Holbrook et al.* [2001], active mantle upwelling is important when crustal thickness is used to infer mantle potential temperature (e.g., Figure 12). The estimate of potential temperature assuming passive upwelling [e.g., *Barton and White*, 1997] may considerably deviate from the actual thermal state of mantle. Although accurate information regarding lower crustal velocity is essential to assess the active upwelling ratio, lower crustal velocity is, unfortunately, generally the least constrained part of crustal structure. The lower crust is characterized by a small vertical velocity gradient, so its velocity structure is constrained mostly with *PmP* travel times. During the 1980s, expanding spread profiling (ESP) using two ships was popular to acquire wide-angle refraction and reflection datafor nearly 1-D geological settings. Because *PmP* phases are usually identifiable only at large offsets when crust is thick [e.g., *Mutter and Zehnder*, 1988], the *PmP* travel time data in an ESP common-midpoint gather, which have a very limited range of ray aperture, does not provide a good constraint on the velocity structure of thick lower crust. The waveform information such as the minimum range of post-critical *PmP* phases was, therefore, commonly used to determine a velocity contrast at the Moho [e.g., *Fowler et al.*, 1989]. Since shallow mantle velocity can be inferred from *Pn* arrivals or its lower limit can be assumed reasonably well, this method seems to be able to derive a lower limit on lower crustal velocity from the waveform information. This approach implicitly assumes, however, that the lower crust can be accurately described as a single block with a uniform velocity or a constant velocity gradient. This may be a dangerous assumption. Because the waveform data are only sensitive to short-wavelength structure [e.g., *Jannane et al.*, 1989], extending a velocity contrast at the Moho to all of the lower crust, whose thickness can be as much as 20 km at LIPs, may not be warranted. For example, the thick transition-zone crust at the southeast Greenland margin exhibits an increase in velocity in the lowermost section (Figure 14c), reducing a velocity contrast at the Moho. The highest crustal velocity observed just above the Moho (~7.4 km s^{-1}) is not representative of average lower crustal velocity.

[42] It is thus preferable to use a tomographic approach with a dense coverage of *PmP* (and *Pn* if available) phases. Because *PmP* travel times are sensitive to both the depth of the Moho and velocity above it, dense ray coverage with a number of source and receiver pairs is required to minimize velocity-depth ambiguity [*Korenaga et al.*, 2000]. We emphasize that velocity-depth ambiguity has a serious influence on the estimate of crustal composition; an error of 3% in velocity, for example, means an error of 0.2 km s^{-1} for 7.0 km s^{-1}, whereas the same degree of uncertainty in the Moho depth has only a trivial effect on the estimate of melt volume. An error of ~0.2 km s^{-1} almost completely nullifies the petrological inference based on crustal velocity (e.g., Figure 12). Except for the tomography of *Korenaga et al.* [2000], however, the issue of velocity-depth ambiguity
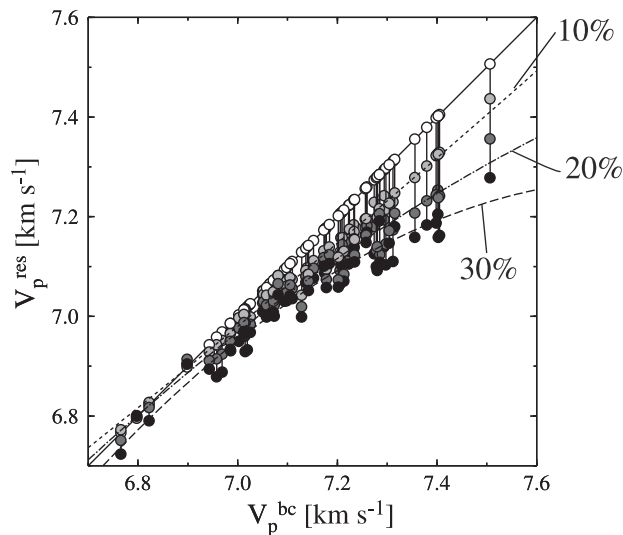
Figure 16. Effect of subcrustal fractionation. P wave velocities of residual phases (V^{res}) formed by fractional crystallization at 1 GPa are plotted as a function of original bulk crustal velocity (V^{bc}), for subcrustal fractionation of 10, 20, and 30%. Results of quadratic regression are $V^{res} = 3.52 + 0.16V + 0.046V^2 (1\sigma = 0.014)$ for $F = 10\%$, $V^{res} = -9.56 + 3.97V - 0.225V^2 (1\sigma = 0.020)$ for $F = 20\%$, and $V^{res} = -22.63 + 7.65V - 0.489V^2 (1\sigma = 0.025)$ for $F = 30\%$.

may not have been properly treated in earlier crustal seismic studies. In addition, a robust uncertainty analysis has rarely been done for published velocity models (see also discussion of *Korenaga et al.* [2000]), whereas placing an error bound on estimated velocity is extremely important for petrological interpretation. The significant difference in lower crustal structure between our transect 2 and other North Atlantic transects (Figure 8), for example, may simply reflect the difference in the quality of original seismic data and the thoroughness of uncertainty analysis.

6.2. Effect of Subcrustal Fractionation

[43] A significant portion of primary melt may crystallize within a mantle column or as ultramafic cumulates at the base of the crust. It is difficult, however, to quantify the amount of this subcrustal fractionation on an observational basis, or predict it from theoretical consideration. Though there are several geochemical studies of the North Atlantic igneous province that indicate relatively high-pressure crystallization [*Morrison et al.*, 1985; *Thompson et al.*, 1986; *Bernstein*, 1994; *Fram and Lesher*, 1997] (0.8–1.5 GPa), such high-pressure fractionation in this area underlain by thick crust could result from deep-crustal or subcrustal fractionation. The possibility of subcrustal fractionation is critical for our bounding approach with the H-V_p diagram, because it is probably the only mechanism, except for residual cracks, that can violate the upper limit on bulk crustal velocity provided by observed lower crustal velocity. Early fractionating phases at high pressures are most likely olivine and clinopyroxene [e.g., *Bender et al.*, 1978; *Presnall et al.*, 1978; *Grove et al.*, 1992; *Langmuir et al.*, 1992], both of which have high seismic velocities, so norm-based bulk crustal velocity can become higher than observed lower

crustal velocity if there is a missing subcrustal component composed of high-velocity minerals.

[44] To quantify this effect, we repeated fractional crystallization modeling at 1 GPa, and compared the bulk crustal velocities of residual liquids with those of primary melts, at several proportions of subcrustal fractionation (Figure 16). The effect of subcrustal fractionation is more significant for higher bulk crustal velocities, and it can be as much as 0.2 km s^{-1}. For bulk crustal velocities lower than 7.0 km s^{-1}, however, its effect is about 0.05 km s^{-1} even for 30% of subcrustal fractionation. This is because plagioclase appears early on fractionation paths for primary liquids corresponding to norm-based bulk crustal velocities less than 7.0 km s^{-1}. On the basis of this modeling, therefore, we conclude that the effect of subcrustal fractionation on the observed low velocity ($\sim$7.0 km s^{-1}) of the thick igneous crust along the southeast Greenland margin is minimal. The possibility of a missing subcrustal component would increase total melt volume and mantle potential temperature, but with a negligible influence on the estimate of active upwelling ratio.

6.3. Effect of Mantle Source Heterogeneity

[45] Our regression of bulk crustal velocity to mantle melting parameters (equation (1)) is only valid for mantle compositions similar to pyrolite model compositions. The majority of abyssal peridotites are best explained as solid residues from the melting of pyrolitic mantle [e.g., *Dick et al.*, 1984; *Kelemen et al.*, 1992; *Asimow*, 1999], and the assumption of pyrolitic source compositions is probably justified for the melting of an average oceanic upper mantle. The local heterogeneity of the mantle source composition is, however, another issue, and the degree of major element heterogeneity and its spatial scale are still poorly known. Whereas isotopic and trace elemental heterogeneity in the convecting upper mantle is firmly established, especially in relation to hot spots, major element heterogeneity is difficult to quantify because the major element compositions of erupted lavas are strongly affected by melting and fractionation processes as well as source compositions. Nonetheless, the importance of major-element source heterogeneity has been suggested for several hot spots including Iceland, Azores, Hawaii, and Yellowstone [e.g., *Langmuir and Hanson*, 1980; *Schilling et al.*, 1983; *Hauri*, 1996; *Takahashi et al.*, 1998; *Korenaga and Kelemen*, 2000]. In particular, based on the major and trace element chemistry of high-MgO lavas, *Korenaga and Kelemen* [2000] suggested that the mantle source for magmatism in much of the North Atlantic province may be relatively Fe-rich compared to the MORB source, with molar Mg/(Mg+Fe) less than 0.87. Such a source could be a mixture of depleted upper mantle and ancient, recycled oceanic crust.

[46] Different mantle source compositions have different solidi and melting functions as well as different melt compositions, and there are too few melting experiments [e.g., *Hirose and Kushiro*, 1993; *Kogiso et al.*, 1998] to develop a quantitative melting model incorporating source heterogeneity. The interpretive method developed in this study, therefore, should be regarded as a baseline, on which we must elaborate to account for source heterogeneity as more data on mantle melting accumulate. To illustrate the potential impact of major-element source heterogeneity on
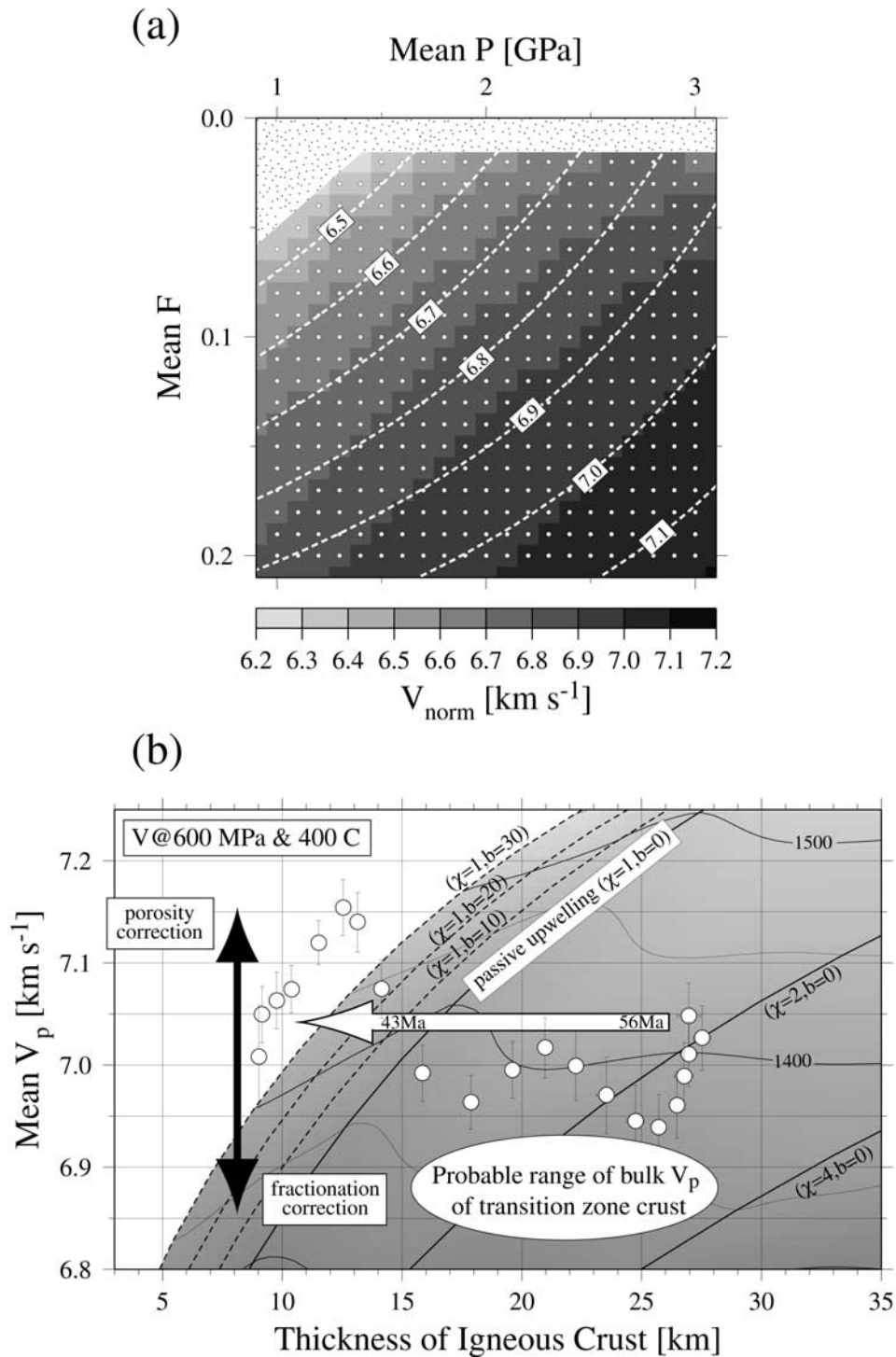
Figure 17. Effect of mantle source heterogeneity. (a) Plot similar to Figure 4a, but for a hypothetical high-Fe mantle composed of 70% depleted pyrolite mantle and 30% MORB. Predicted velocity based on equation (12) is shown as dashed contour. (b) Alternative H-V_p diagram based on equation (12), lower mantle solidus, and higher melting rate (see text for details). Open circles with error bars denote transect 2 seismic data as in Figure 15c.

our interpretation, however, we constructed an alternative H-V_p diagram corresponding to a hypothetical source mantle that is comprised of 70% depleted pyrolite mantle and 30% MORB (with whole rock Mg# of 0.86). We emphasize that this is a highly preliminary attempt, solely to provide

some quantitative basis for our discussion. The depleted mantle and MORB compositions are from *Kinzler* [1997] and *Hofmann* [1988], respectively. We used the method of *Kinzler* [1997] to calculate isobaric batch melts for pressures of 1–3 GPa and melt fractions up to 0.20. Some melt

compositions at low melt fractions seem to be the result of unstable extrapolation from the experimentally constrained compositional space, but they are retained in the following to maximize the number of available data. Corresponding norm-based velocity is calculated, and the relation between norm-based velocity and melting parameters is obtained by linear regression as

$$V(P, F) = 6.024 + 0.26P + 3.73F - 0.70PF \qquad (12)$$

which has one standard deviation of about 0.03 km s^{-1} (Figure 17a). More elaborate regression, such as that used for equation (1), is not warranted here because of our limited understanding of melting of non-pyrolitic mantle. The slopes of the mantle solidus and adiabat are set as in equations (4) and (5), but the solidus is decreased by 60°C to reflect the Fe enrichment. A linear melting function of equation (6) is employed with of 18%/GPa (i.e., 50% increase over our standard melting rate, 12%/GPa) [e.g., *Hirschmann and Stolper*, 1996]. With these modifications, appropriate for the change in source mantle composition, a new H-V_p diagram is constructed (Figure 17b). The data from thick (>15 km) igneous crust on SIGMA transect 2 off southeast Greenland now fall in the moderately active upwelling regime ($\chi = 1 - 3$). Considering that bulk crustal velocity can be lower than the observed lower crustal velocity by 0.15 km s^{-1}, the overall intensity of active upwelling may be slightly higher, but it is probably less than $\chi = 4$. On the other hand, the data from thinner, oceanic crust is hard to interpret using this H-V_p diagram, since it apparently requires a thick lithospheric lid. We speculate that the compositional anomaly in the mantle source in this area was significant only during the first 10 m.y. of rifting. A temporal transition in source composition may explain the sharp increase in crustal velocity observed around km 250 on transect 2 (Figure 15). Whereas mantle potential temperature may have been continuously close to normal and the active upwelling of mantle may have gradually decreased since the onset of rifting, the existence of intrinsic chemical heterogeneity and its sudden exhaustion may be the main cause for the formation of thick, low-velocity, igneous crust on the southeast Greenland margin.

7. Conclusion

[47] We developed a new method to relate the seismic crustal structure of large igneous provinces with the process of mantle melting. Following the approach taken by *Kelemen and Holbrook* [1995], we first established a relation between bulk crustal velocity and mantle melting parameters including the pressure and degree of melting, based on an extended database of mantle melting experiments. A more accurate calculation of velocity from a given composition through the CIPW norm results in a much tighter relation than that of KH95, with one standard deviation of only 0.05 km s^{-1}. Noting that upper crustal velocity does not contain useful petrological information, and that it is impossible to uniquely determine a bulk crustal composition from lower crustal velocity alone, we estimated the possible range of compositional variations in the lower crust during crustal accretion by modeling fractional crystallization at a range of pressures. On the basis of the results of this

crystallization modeling, a bound on the possible range of bulk crustal velocity for a given lower crustal velocity was obtained as a function of the proportion of lower crust within the total igneous crust. We found that the seismic structure of normal oceanic crust imposes a problem in its petrological interpretation based on a standard melting model, unless the effects of residual crack porosity are considered. Finally, a simple mantle melting model was developed to illustrate the effects of active mantle upwelling and a preexisting lithospheric lid, which are prominent complicating factors in the formation of large igneous provinces, and a relationship between mantle melting parameters and corresponding seismic observables was succinctly summarized in a single H-V_p diagram.

[48] We illustrated the practical use of our method, using an example from the southeast Greenland margin, to estimate the past mantle dynamics during the opening of the North Atlantic. The preliminary conclusions of *Korenaga et al.* [2000] were reinforced with this new method; thick (~30 km) igneous crust with an average lower crustal velocity of ~7.0 km s^{-1} is the result of active upwelling of mantle with almost normal potential temperature. Using this example, we also discussed possible, additional complications such as subcrustal fractionation and variable mantle source compositions. The effect of major element heterogeneity in a mantle source composition is the most significant remaining uncertainty when inferring mantle melting dynamics from the seismic structure of igneous crust.

References

Ahern, J. L., and D. L. Turcotte, Magma migration beneath an ocean ridge, *Earth Planet. Sci. Lett.*, *45*, 115–122, 1979.

Anderson, D. L., Superplumes or supercontinents?, *Geology*, *22*, 39–42, 1994.

Asimow, P. D., A model that reconciles major- and trace-element data from abyssal peridotites, *Earth Planet. Sci. Lett.*, *169*, 303–319, 1999.

Asimow, P. D., M. M. Hirschmann, and E. M. Stolper, An analysis of variations in isentropic melt productivity, *Philos. Trans. R. Soc. London, Ser. A*, *355*, 255–281, 1997.

Baker, M. B., and E. M. Stolper, Determining the composition of high-pressure mantle melts using diamond aggregates, *Geochim. Cosmochim. Acta*, *58*, 2811–2827, 1994.

Barnouin-Jha, K., E. M. Parmentier, and D. W. Sparks, Buoyant mantle upwelling and crustal production at oceanic spreading centers: On-axis segmentation and off-axis melting, *J. Geophys. Res.*, *102*, 11,979–11,989, 1997.

Barton, A. J., and R. S. White, Crustal structure of Edoras Bank continental margin and mantle thermal anomalies beneath the North Atlantic, *J. Geophys. Res.*, *102*, 3109–3129, 1997.

Bender, J. F., F. N. Hodges, and A. E. Bence, Petrogenesis of basalts from the project FAMOUS area: Experimental study from 0 to 15 kbars, *Earth Planet. Sci. Lett.*, *41*, 277–302, 1978.

Bernstein, S., High-pressure fractionation in rift-related basaltic magmatism: Faeroe plateau basalts, *Geology*, *22*, 815–818, 1994.

Berryman, J. G., Mixture theories for rock properties, in *Rock Physics and Phase Relations: A Handbook of Physical Constants, AGU Ref. Shelf*, vol. 3, edited by T. J. Ahrens, pp. 205–228, AGU, Washington, D. C., 1995.

Birch, F., The velocity of compressional waves in rocks to 10 kilobars, part 2, *J. Geophys. Res.*, 66, 2199–2224, 1961.

Bottinga, Y., and D. F. Weill, Densities of liquid silicate systems calculated from partial molar volumes of oxide components, *Am. J. Sci.*, 269, 169–182, 1970.

Boudier, F., A. Nicolas, and B. Ildefonse, Magma chambers in the oman ophiolite: Fed from the top or the bottom?, *Earth Planet. Sci. Lett.*, 144, 239–250, 1996.

Boutilier, R. R., and C. E. Keen, Small-scale convection and divergent plate boundaries, *J. Geophys. Res.*, 104, 7389–7403, 1999.

Braun, M. G., G. Hirth, and E. M. Parmentier, The effects of deep damp melting on mantle flow and melt generation beneath mid-ocean ridges, *Earth Planet. Sci. Lett.*, 176, 339–356, 2000.

Cannat, M., How thick is the magmatic crust at slow spreading oceanic ridges?, *J. Geophys. Res.*, 101, 2847–2857, 1996.

Chen, Y., A second melt lens at fast spreading mid-ocean ridges? (abstract), *Eos Trans. AGU*, 79(45), Fall Meet. Suppl., F837, 1998.

Christensen, N. I., Compressional wave velocities in possible mantle rocks to pressures of 30 kilobars, *J. Geophys. Res.*, 79, 407–412, 1974.

Christensen, N. I., Compressional wave velocities in rocks at high temperatures and pressures, critical thermal gradients, and crustal low-velocity zones, *J. Geophys. Res.*, 84, 6849–6857, 1979.

Christensen, N. I., and W. D. Mooney, Seismic velocity structure and composition of the continental crust: A global view, *J. Geophys. Res.*, 100, 9761–9788, 1995.

Christensen, N. I., and M. H. Salisbury, Structure and constitution of the lower oceanic crust, *Rev. Geophys.*, 13, 57–86, 1975.

Christensen, N. I., and G. H. Shaw, Elasticity of mafic rocks from the Mid-Atlantic Ridge, *Geophys. J. R. Astron. Soc.*, 20, 271–284, 1970.

Christensen, N. I., and J. D. Smewing, Geology and seismic structure of the northern section of the Oman ophiolite, *J. Geophys. Res.*, 86, 2545–2555, 1981.

Coffin, M. F., and O. Eldholm, Large igneous provinces: Crustal structure, dimensions, and external consequences, *Rev. Geophys.*, 32, 1–36, 1994.

Cordery, M. J., and J. Phipps Morgan, Convection and melting at mid-ocean ridges, *J. Geophys. Res.*, 98, 19,477–19,503, 1993.

Daines, M. J., and F. M. Richter, An experimental method for directly determining the interconnectivity of melt in a partially molten system, *Geophys. Res. Lett.*, 15, 1459–1462, 1988.

DePaolo, D. J., Trace element and isotopic effects of combined wallrock assimilation and fractional crystallization, *Earth Planet. Sci. Lett.*, 53, 189–202, 1981.

Detrick, R., J. Collins, R. Stephen, and S. Swift, In situ evidence for the nature of the seismic layer 2/3 boundary in oceanic crust, *Nature*, 370, 288–290, 1994.

Dick, H. J. B., R. L. Fisher, and W. B. Bryan, Mineralogic variability of the uppermost mantle along mid-ocean ridges, *Earth Planet. Sci. Lett.*, 69, 88–106, 1984.

Dick, H. J. B., P. S. Meyer, S. Bloomer, S. Kirby, D. Stakes, and C. Mawer, Lithostratigraphic evolution of an in-situ section of oceanic layer 3, *Proc. Ocean Drill. Program Sci. Results*, 118, 439–538, 1991.

Dick, H. J. B., P. T. Robinson, and P. S. Meyer, The plutonic foundation of a slow-spreading ridge, in *Synthesis of Results from Scientific Drilling in the Indian Ocean*, *Geophys. Monogr. Ser.*, vol. 70, edited by R. A. Duncan et al., pp. 1–39, AGU, Washington, D. C., 1992.

Farnetani, C. G., M. A. Richards, and M. S. Ghiorso, Petrological models of magma evolution and deep crustal structure beneath hotspots and flood basalt provinces, *Earth Planet. Sci. Lett.*, 143, 81–94, 1996.

Fowler, S. R., R. S. White, G. D. Spence, and G. K. Westbrook, The Hatton Bank continental margin, II, Deep structure from two-ship expanding spread seismic profiles, *Geophys. J.*, 96, 295–309, 1989.

Fram, M. S., and C. E. Lesher, Geochemical constraints on mantle melting during creation of the North Atlantic basin, *Nature*, 363, 712–715, 1993.

Fram, M. S., and C. E. Lesher, Generation and polybaric differentiation of east Greenland early Tertiary flood basalts, *J. Petrol.*, 38, 231–275, 1997.

Gillis, K. M., C. Mével, J. F. Allan, and the Shipboard Scientific Party, *Proceedings of the Drilling Program, Initial Report*, vol. 147, Ocean Drill. Program, College Station, Tex., 1993.

Gregory, R. T., and H. P. Taylor, An oxygen isotope profile in a section of Cretaceous oceanic crust, Samail ophiolite, Oman: Evidence for d^{18}O buffering of the oceans by deep (>5 km) seawater-hydrothermal circulation at mid-ocean ridges, *J. Geophys. Res.*, 86, 2737–2755, 1981.

Grove, T. L., R. J. Kinzler, and W. B. Bryan, Fractionation of mid-ocean ridge basalt (MORB), in *Mantle Flow and Melt Generation at Mid-Ocean Ridges*, *Geophys. Monogr. Ser.*, vol. 71, edited by J. P. Morgan, D. K. Blackman, and J. M. Sinton, pp. 281–310, AGU, Washington, D. C., 1992.

Hart, S. R., and A. Zindler, In search of a bulk-earth composition, *Chem. Geol.*, 57, 247–267, 1986.

Hashin, Z., and S. Shtrikman, A variational approach to the elastic behavior of multiphase materials, *J. Mech. Phys. Solids*, 11, 127–140, 1963.

Hauri, E. H., Major-element variability in the Hawaiian mantle plume, *Nature*, 382, 415–419, 1996.

Henstock, T. J., A. W. Woods, and R. S. White, The accretion of oceanic crust by episodic sill intrusion, *J. Geophys. Res.*, 98, 4143–4161, 1993.

Hill, R. I., I. H. Campbell, G. F. Davies, and R. W. Griffiths, Mantle plumes and continental tectonics, *Science*, 256, 186–193, 1992.

Hirose, K., and I. Kushiro, Partial melting of dry peridotites at high pressures: Determination of compositions of melts segregated from peridotite using aggregates of diamond, *Earth Planet. Sci. Lett.*, 114, 477–489, 1993.

Hirschmann, M. M., and E. M. Stolper, A possible role for garnet pyroxenite in the origin of the "garnet signature" in MORB, *Contrib. Mineral. Petrol.*, 124, 185–208, 1996.

Hofmann, A. W., Chemical differentiation of the Earth: The relationship between mantle, continental crust, and oceanic crust, *Earth Planet. Sci. Lett.*, 90, 297–314, 1988.

Holbrook, W. S., and P. B. Kelemen, Large igneous province on the US Atlantic margin and implications for magmatism during continental breakup, *Nature*, 364, 433–436, 1993.

Holbrook, W. S., et al., Mantle thermal structure and melting processes during continental breakup in the North Atlantic, *Earth Planet. Sci. Lett.*, 190, 251–266, 2001.

Ito, G., J. Lin, and C. W. Gable, Dynamics of mantle flow and melting at a ridge-centered hotspot: Iceland and the Mid-Atlantic Ridge, *Earth Planet. Sci. Lett.*, 144, 53–74, 1996.

Iturrino, G. J., N. I. Christensen, S. Kirby, and M. H. Salisbury, Seismic velocities and elastic properties of oceanic gabbroic rocks from Hole 735B, *Proc. Ocean Drill. Program Sci. Results*, 118, 227–244, 1991.

Iturrino, G. J., D. J. Miller, and N. I. Christensen, Velocity behavior of lower crustal and upper mantle rocks from a fast-spreading ridge at Hess Deep, *Proc. Ocean Drill. Program Sci. Results*, 147, 417–440, 1996.

Jackson, I., R. L. Rudnick, S. Y. O'Reilly, and C. Bezant, Measured and calculated elastic wave velocities for xenoliths from the lower crust and upper mantle, *Tectonophysics*, 173, 207–210, 1990.

Jannane, M., et al., Wavelengths of earth structures that can be resolved from seismic reflection data, *Geophysics*, 54, 906–910, 1989.

Johnson, K. T. M., H. J. B. Dick, and N. Shimizu, Melting in the oceanic upper mantle: An ion microprobe study of diopsides in abyssal peridotites, *J. Geophys. Res.*, 95, 2661–2678, 1990.

Keen, C. E., and R. R. Boutilier, Lithosphere-asthenosphere interactions below rifts, in *Rifted Ocean-Continent Boundaries*, edited by E. Banda, M. Talwani, and M. Torne, pp. 17–30, Kluwer Acad., Norwell, Mass., 1995.

Kelemen, P. B., and E. Aharonov, Periodic formation of magma fractures and generation of layered gabbros in the lower crust beneath oceanic spreading centers, in *Faulting and Magmatism at Mid-Ocean Ridges*, *Geophys. Monogr. Ser.*, vol. 106, edited by W. R. Buck et al., pp. 267–289, AGU, Washington, D. C., 1998.

Kelemen, P. B., and W. S. Holbrook, Origin of thick, high-velocity igneous crust along the U.S. East Coast margin, *J. Geophys. Res.*, 100, 10,077–10,094, 1995.

Kelemen, P. B., H. J. B. Dick, and J. E. Quick, Formation of harzburgite by pervasive melt/rock reaction in the upper mantle, *Nature*, 358, 635–641, 1992.

Kelemen, P. B., N. Shimizu, and V. J. M. Salters, Extraction of mid-ocean-ridge basalt from the upwelling mantle by focused flow of melt in dunite channels, *Nature*, 375, 747–753, 1995.

Kelemen, P. B., G. Hirth, N. Shimizu, M. Spiegelman, and H. J. B. Dick, A review of melt migration processes in the adiabatically upwelling mantle beneath oceanic spreading ridges, *Philos. Trans. R. Soc. London, Ser. A*, 355, 283–318, 1997a.

Kelemen, P. B., K. Koga, and N. Shimizu, Geochemistry of gabbro sills in the crust/mantle transition zone of the Oman ophiolite: Implications for the origin of the oceanic lower crust, *Earth Planet. Sci. Lett.*, 146, 475–488, 1997b.

Kern, H., and J. M. Tubia, Pressure and temperature dependence of *P*- and *S*-wave velocities, seismic anisotropy and density of sheared rocks from the Sierra Alpujata massif (Ronda peridotites, southern Spain), *Earth Planet. Sci. Lett.*, 119, 191–205, 1993.

Kinzler, R. J., Melting of mantle peridotite at pressures approaching the spinel to garnet transition: Application to mid-ocean ridge basalt petrogenesis, *J. Geophys. Res.*, 102, 852–874, 1997.

Kinzler, R. J., and T. L. Grove, Primary magmas of mid-ocean ridge basalts, 2. Applications, *J. Geophys. Res.*, 97, 6907–6926, 1992.

Kinzler, R. J., and T. L. Grove, Corrections and further discussion of the primary magmas of mid-ocean ridge basalts, 1 and 2, *J. Geophys. Res.*, 98, 22,339–22,347, 1993.

Klein, E. M., and C. H. Langmuir, Global correlations of ocean ridge basalt

chemistry with axial depth and crustal thickness, *J. Geophys. Res.*, *92*, 8089–8115, 1987.

Kogiso, T., K. Hirose, and E. Takahashi, Melting experiments on homogeneous mixtures of peridotite and basalt: Application to the genesis of ocean island basalts, *Earth Planet. Sci. Lett.*, *162*, 45–61, 1998.

Korenaga, J., and T. H. Jordan, On the state of sublithospheric upper mantle beneath a supercontinent, *Geophys. J. Int.*, *149*, 179–189, 2002.

Korenaga, J., and P. B. Kelemen, Melt migration through the oceanic lower crust: A constraint from melt percolation modeling with finite solid diffusion, *Earth Planet. Sci. Lett.*, *156*, 1–11, 1998.

Korenaga, J., and P. B. Kelemen, Major element heterogeneity of the mantle source in the North Atlantic igneous province, *Earth Planet. Sci. Lett.*, *184*, 251–268, 2000.

Korenaga, J., W. S. Holbrook, G. M. Kent, P. B. Kelemen, R. S. Detrick, H. C. Larsen, J. R. Hopper, and T. Dahl-Jensen, Crustal structure of the southeast Greenland margin from joint refraction and reflection seismic tomography, *J. Geophys. Res.*, *105*, 21,591–21,614, 2000.

Korenaga, J., W. S. Holbrook, R. S. Detrick, and P. B. Kelemen, Gravity anomalies and crustal structure at the southeast Greenland margin, *J. Geophys. Res.*, *106*, 8853–8876, 2001.

Kuster, G. T., and M. N. Toksöz, Velocity and attenuation of seismic waves in two-phase media, part I, Theoretical formulations, *Geophysics*, *39*, 587–606, 1974.

Langmuir, C. H., Geochemical consequences of in situ crystallization, *Nature*, *340*, 199–205, 1989.

Langmuir, C. H., and G. N. Hanson, An evaluation of major element heterogeneity in the mantle sources of basalts, *Philos. Trans. R. Soc. London, Ser. A*, *297*, 383–407, 1980.

Langmuir, C. H., E. M. Klein, and T. Plank, Petrological systematics of mid-ocean ridge basalts: Constraints on melt generation beneath ocean ridges, in *Mantle Flow and Melt Generation at Mid-Ocean Ridges*, *Geophys. Monogr. Ser.*, vol. 71, edited by J. P. Morgan, D. K. Blackman, and J. M. Sinton, pp. 183–280, AGU, Washington, D. C., 1992.

Lister, C. R. B., On the penetration of water into hot rock, *Geophys. J. R. Astron. Soc.*, *39*, 465–509, 1974.

Lister, C. R. B., The basic physics of water penetration into hot rocks, in *Hydrothermal Processes at Seafloor Spreading Centers*, pp. 141–168, Plenum, New York, 1983.

Lundstrom, C. C., J. Gill, Q. Williams, and M. R. Perfit, Mantle melting and basalt extraction by equilibrium porous flow, *Science*, *270*, 1958–1961, 1995.

Manning, C. E., and C. J. MacLeod, Fracture-controlled metamorphism of Hess Deep gabbros, Site 894: Constraints on the roots of mid-ocean ridge hydrothermal systems at fast-spreading centers, *Proc. Ocean Drill. Program Sci. Results*, *147*, 189–212, 1996.

Mavko, G., T. Mukerji, and J. Dvorkin, *The Rock Physics Handbook*, Cambridge Univ. Press, New York, 1998.

McDonough, W. F., and S.-S. Sun, The composition of the Earth, *Chem. Geol.*, *120*, 223–253, 1995.

McKenzie, D., The generation and compaction of partially molten rock, *J. Petrol.*, *25*, 713–765, 1984.

McKenzie, D., and M. J. Bickle, The volume and composition of melt generated by extension of the lithosphere, *J. Petrol.*, *29*, 625–679, 1988.

Menke, W., and D. Sparks, Crustal accretion model for Iceland predicts 'cold' crust, *Geophys. Res. Lett.*, *22*, 1673–1676, 1995.

Morgan, J. V., P. J. Barton, and R. S. White, The Hatton Bank continental margin, III, Structure from wide-angle OBS and multichannel seismic refraction profiles, *Geophys. J.*, *96*, 367–384, 1989.

Morrison, M. A., R. N. Thompson, and A. P. Dickin, Geochemical evidence for complex magmatic plumbing during development of a continental volcanic center, *Geology*, *13*, 581–584, 1985.

Mutter, C. Z., and J. C. Mutter, Variations in thickness of layer 3 dominate oceanic crustal structure, *Earth Planet. Sci. Lett.*, *117*, 295–317, 1993.

Mutter, J. C., and C. M. Zehnder, Deep crustal structure and magmatic processes: The inception of seafloor spreading in the Norwegian-Greenland sea, in *Early Tertiary Volcanism and the Opening of the NE Atlantic*, edited by A. C. Morton and L. M. Parson, *Geol. Soc. Spec. Publ.*, *39*, 35–48, 1988.

Mutter, J. C., W. R. Buck, and C. M. Zehnder, Convective partial melting, 1, A model for the formation of thick basaltic sequences during the initiation of spreading, *J. Geophys. Res.*, *93*, 1031–1048, 1988.

Nicolas, A., I. Reuber, and K. Benn, A new magma chamber model based on structural studies in the Oman ophiolite, *Tectonophysics*, *151*, 87–105, 1988.

O'Hara, M. J., Geochemical evolution during fractional crystallisation of a periodically refilled magma chamber, *Nature*, *266*, 503–507, 1977.

Pallister, J. S., and C. A. Hopson, Samail Ophiolite plutonic suite: Field relations, phase variation, cryptic variation and layering, and a model of a spreading ridge magma chamber, *J. Geophys. Res.*, *86*, 2593–2644, 1981.

Philpotts, A. R., *Principles of Igneous and Metamorphic Petrology*, Prentice-Hall, Old Tappan, N. J., 1990.

Phipps Morgan, J., and Y. J. Chen, The genesis of oceanic crust: Magma injection, hydrothermal circulation, and crustal flow, *J. Geophys. Res.*, *98*, 6283–6297, 1993.

Plank, T., and C. H. Langmuir, Effects of the melting regime on the composition of the oceanic crust, *J. Geophys. Res.*, *97*, 19,749–19,770, 1992.

Plank, T., M. Spiegelman, C. H. Langmuir, and D. W. Forsyth, The meaning of "mean F": Clarifying the mean extent of melting at ocean ridges, *J. Geophys. Res.*, *100*, 15,045–15,052, 1995.

Presnall, D. C., S. A. Dixon, T. H. O'Donnell, N. L. Brenner, R. L. Schrock, and D. W. Dycus, Liquidus phase relations on the join diopside-forsterite-anorthite from 1 atm to 20 kbar: Their bearing on the generation and crystallization of basaltic magma, *Contrib. Mineral. Petrol.*, *66*, 203–220, 1978.

Quick, J. E., and R. P. Denlinger, Ductile deformation and the origin of layered gabbro in ophiolites, *J. Geophys. Res.*, *98*, 14,015–14,027, 1993.

Rabinowicz, M., G. Ceuleneer, and A. Nicolas, Melt segregation and flow in mantle diapirs below spreading centers: Evidence from the Oman ophiolite, *J. Geophys. Res.*, *92*, 3475–3486, 1987.

Raitt, R. W., The crustal rocks, in *The Sea*, vol. 3, edited by M. N. Hill, pp. 85–102, Wiley-Interscience, New York, 1963.

Ribe, N. M., U. R. Christensen, and J. Theiing, The dynamics of plume-ridge interaction, 1, Ridge-centered plumes, *Earth Planet. Sci. Lett.*, *134*, 155–168, 1995.

Richards, M. A., R. A. Duncan, and V. E. Courtillot, Flood basalts and hotspot tracks: Plume heads and tails, *Science*, *246*, 103–107, 1989.

Ringwood, A. E., *Compositions and Petrology of the Earth's Mantle*, McGraw-Hill, New York, 1975.

Robinson, P. T., R. P. Von Herzen, A. C. Adamson, and the Shipboard Scientific Party, *Proceedings of the Drilling Program Initial Report*, vol. 118, Ocean Drill. Program, College Station, Tex., 1987.

Schilling, J. G., M. Zajac, R. Evans, T. Johnson, W. White, J. D. Devine, and R. Kingsley, Petrologic and geochemical variations along the Mid-Atlantic Ridge from 29°N to 73°N, *Am. J. Sci.*, *283*, 510–586, 1983.

Scott, D. R., Small-scale convection and mantle melting beneath mid-ocean ridges, in *Mantle Flow and Melt Generation at Mid-Ocean Ridges*, *Geophys. Monogr. Ser.*, vol. 71, edited by J. P. Morgan, D. K. Blackman, and J. M. Sinton, pp. 327–352, AGU, Washington, D. C., 1992.

Shor, G. G., Jr., H. W. Menard, and R. S. Raitt, Structure of the Pacific Basin, in *The Sea*, vol. 4, edited by A. E. Maxwell, pp. 3–27, Wiley-Interscience, New York, 1970.

Sinton, J. M., and R. S. Detrick, Mid-ocean ridge magma chambers, *J. Geophys. Res.*, *97*, 197–216, 1992.

Sleep, N. H., Hydrothermal circulation, anhydrite precipitation, and thermal structure at ridge axes, *J. Geophys. Res.*, *96*, 2375–2387, 1991.

Sobolev, A. V., and N. Shimizu, Ultra-depleted primary melt included in an olivine from the Mid-Atlantic Ridge, *Nature*, *363*, 151–154, 1993.

Sobolev, S. V., and A. Y. Babeyko, Modeling of mineralogical composition, density and elastic wave velocities in anhydrous magmatic rocks, *Surv. Geophys.*, *15*, 515–544, 1994.

Sparks, R. S. J., P. Meyer, and H. Sigurdsson, Density variation amongst mid-ocean ridge basalts: Implications for magma mixing and the scarcity of primitive lavas, *Earth Planet. Sci. Lett.*, *46*, 419–430, 1980.

Spiegelman, M., Geochemical consequences of melt transport in 2-D: The sensitivity of trace elements to mantle dynamics, *Earth Planet. Sci. Lett.*, *118*, 115–132, 1996.

Spudich, P., and J. Orcutt, A new look at the seismic velocity structure of the oceanic crust, *Rev. Geophys.*, *18*, 627–645, 1980.

Stolper, E., and D. Walker, Melt density and the average composition of basalt, *Contrib. Mineral. Petrol.*, *74*, 7–12, 1980.

Su, W., and W. R. Buck, Buoyancy effects on mantle flow under mid-ocean ridges, *J. Geophys. Res.*, *98*, 12,191–12,205, 1993.

Tackley, P. J., and D. Stevenson, A mechanism for spontaneous self-perpetuating volcanism on the terrestorial planets, in *Flow and Creep in the Solar System: Observations, Modeling and Theory*, edited by D. B. Stone and S. K. Runcorn, pp. 307–321, Kluwer Acad., Norwell, Mass., 1993.

Takahashi, E., and I. Kushiro, Melting of a dry peridotite at high pressures and basalt magma genesis, *Am. Mineral.*, *68*, 859–879, 1983.

Takahashi, E., K. Nakajima, and T. L. Wright, Origin of the Columbia River basalts: Melting model of a heterogeneous plume head, *Earth Planet. Sci. Lett.*, *162*, 63–80, 1998.

Thompson, R. N., M. A. Morrison, A. P. Dickin, L. L. Gibson, and R. S. Harmon, Two contrasting styles of interaction between basic magma and continental crust in the British Tertiary Volcanic Province, *J. Geophys. Res.*, *91*, 5985–5997, 1986.

Turcotte, D. L., and J. P. Morgan, The physics of magma migration and mantle flow beneath a mid-ocean ridge, in *Mantle Flow and Melt Generation at Mid-Ocean Ridges*, *Geophys. Monogr. Ser.*, vol. 71, edited by

J. P. Morgan, D. K. Blackman, and J. M. Sinton, pp. 155–182, AGU, Washington, D. C., 1992.

Walter, M. J., Melting of garnet peridotite and the origin of komatiite and depleted lithosphere, *J. Petrol.*, *39*, 29–60, 1998.

Watt, J. P., G. F. Davies, and R. J. O'Connell, The elastic properties of composite minerals, *Rev. Geophys.*, *14*, 541–563, 1976.

Weaver, J. S., and C. H. Langmuir, Calculation of phase equilibrium in mineral-melt systems, *Comput. Geosci.*, *16*, 1–19, 1990.

White, R., and D. McKenzie, Magmatism at rift zones: The generation of volcanic continental margins and flood basalts, *J. Geophys. Res.*, *94*, 7685–7729, 1989.

White, R. S., and D. McKenzie, Mantle plumes and flood basalts, *J. Geophys. Res.*, *100*, 17,543–17,585, 1995.

White, R. S., G. D. Spence, S. R. Fowler, D. P. McKenzie, G. K. Westbrook, and A. N. Bowen, Magmatism at rifted continental margins, *Nature*, *330*, 439–444, 1987.

White, R. S., D. McKenzie, and R. K. O'Nions, Oceanic crustal thickness from seismic measurements and rare earth element inversions, *J. Geophys. Res.*, *97*, 19,683–19,715, 1992.

Wilkens, R. H., G. J. Fryer, and J. Karsten, Evolution of porosity and seismic structure of upper oceanic crust: Importance of aspect ratios, *J. Geophys. Res.*, *96*, 17,981–17,995, 1991.

Zehnder, C. M., J. C. Mutter, and P. Buhl, Deep seismic and geochemical constraints on the nature of rift-induced magmatism during breakup of the North Atlantic, *Tectonophysics*, *173*, 545–565, 1990.

————————

W. S. Holbrook, Department of Geology and Geophysics, University of Wyoming, P.O. Box 3006, Laramie, WY 82071-3006, USA. (steveh@uwyo.edu)

P. B. Kelemen, Department of Geology and Geophysics, Woods Hole Oceanographic Institution, MS8/McLean Lab, Woods Hole, MA 02543, USA. (peterk@whoi.edu)

J. Korenaga, Department of Earth and Planetary Science, 377 McCone Hall, University of California, Berkeley, CA 94720-4767, USA. (korenaga@seismo.berkeley.edu)